# Effects of Febuxostat on Autistic Behaviors and Computational Investigations of Diffusion and Pharmacokinetics

Jamelle M. Simmons

Dissertation submitted to the Faculty of the

Virginia Polytechnic Institute and State University

in partial fulfillment of the requirements for the degree of

Doctor of Philosophy

in

Biomedical Engineering

Yong W. Lee, Chair

Luke E. Achenie

Hampton C. Gabler

Alexei Morozov

Aaron S. Goldstein

John H. Rossmeisl

November 27, 2018

Blacksburg, Virginia

Keywords: Autism Spectrum Disorder, Xanthine Oxidase, Reactive Oxygen Species, Pharmacokinetics, Animal Behavior

# Effects of Febuxostat on Autistic Behaviors and Computational Investigations of Diffusion and Pharmacokinetics

Jamelle M. Simmons

(ABSTRACT)

Autism spectrum disorder (ASD) is a lifelong disability that has seen a rise in prevalence from 1 in 150 children to 1 in 59 between 2000 and 2014. Patients show behavioral abnormalities in the areas of social interaction, communication, and restrictive and repetitive behaviors. As of now, the exact cause of ASD is unknown and literature points to multiple causes. The work contained within this dissertation explored the reduction of oxidative stress in brain tissue induced by xanthine oxidase (XO). Febuxostat is a new FDA approved XO-inhibitor that has been shown to be more selective and potent than allopurinol in patients with gout.The first study developed a computational model to calculate an effective diffusion constant ($D_{eff}$) of lipophilic compounds, such as febuxostat, that can cross endothelial cells of the blood-brain barrier (BBB) by the transcellular pathway. In the second study, male juvenile autistic (BTBR) mice were treated with febuxostat for seven days followed by behavioral testing and quantification of oxidative stress in brain tissue compared to controls.

Results of the first study showed that the lipophilic tracer chosen, as a substitute for febuxostat, could be modeled under the assumption of passive diffusion while experimental controls did not fit this model. The second study revealed no significant differences between BTBR mice that received febuxostat or the drug vehicle in both behavioral testing and quantification of oxidative stress in brain tissue. In the final study, of the four models proposed, one model was selected as the most plausible that considered transport into the CNS. As there is currently no literature surrounding tissue and organ ADME for febuxostat the final proposed model would need to be updated as new information becomes available.

# Effects of Febuxostat on Autistic Behaviors and Computational Investigations of Diffusion and Pharmacokinetics

Jamelle M. Simmons

(GENERAL AUDIENCE ABSTRACT)

Autism spectrum disorder (ASD) is a lifelong disability that has seen a rise in prevalence from 1 in 150 children to 1 in 59 between 2000 and 2014. Patients show behavioral abnormalities in the areas of (1) social interaction, how an individual acts and reacts to others around them, (2) communication, the use of and understanding of language and facial expressions, and (3) restrictive and repetitive behaviors where individuals may have focused interests on specific topics/subjects and stick to set routines. As of now, the exact cause of ASD is unknown and literature points to multiple causes. The work contained within this dissertation explored the reduction of oxidative stress in brain tissue induced by the enzyme xanthine oxidase (XO). Oxidative stress is noted as the imbalance between free radicals (pro-oxidant) and antioxidant defenses where the pro-oxidant levels are greater than the antioxidant defenses leading to cell and tissue damage. Febuxostat is a new FDA approved XO-inhibitor that has been shown to target and inhibit XO better than allopurinol (an older XO-inhibitor) in patients with gout.

The first study developed a computational model to calculate an effective diffusion constant ($D_{eff}$) that explained the free movement of a compound (substance) across cells, also known as trancellular movement. The transcellular pathway is the direct movement of compounds into a cell that requires no additional cellular energy or specialized transport routes to get the compounds into the cell. In the second study, male juvenile autistic (BTBR) mice were treated with febuxostat for seven days followed by behavioral testing to study social interaction and restrictive and repetitive behaviors in autistic mice compared to non-

autistic mice. Next, oxidative stress levels were measured in the brain tissue of autistic mice and compared to non-autistic mice. The third study developed four hypothesis-based human pharmacokinetic (PK) multi-compartment models of drug absorption, distribution, metabolism, and excretion (ADME). Pharmacokinetics is the study of what the body does to a drug once it is given, i.e how it gets into the bloodstream, where it goes in the body, how it is broken down, and how it is removed from the body . Compartments in PK models can be used to represent parts of the body such as blood, tissues, and organs.

Results of the first study showed that the compound chosen as a substitute for febuxostat could be modeled under the assumption of passive diffusion, free movement across cells without use of energy or specialized routes, while the other compounds did not fit this model. The second study revealed no significant differences between autistic (BTBR) mice, those that received febuxostat treatment, and non-autistic mice for behavioral testing and oxidative stress levels in brain tissue. In the final study, of the four models proposed, one model was selected as the most plausible that considered drug movement into the brain and spinal cord regions. As there is currently no literature surrounding tissue and organ ADME for febuxostat the final proposed model would need to be updated as new information becomes available.

# Dedication

*I dedicate this dissertation to Dr. Stephanie Sullivan, my family, and especially my parents, Norman and Wyanette Simmons, who have been supportive advocates through my undergraduate to doctoral journey.*

*To Dr. Sullivan, thank you for offering me the opportunity to be involved in research as an undergraduate at East Carolina University, research and graduate school never crossed as I had originally planned for a career in industry shorty after graduating. You helped mold me into an independent student by giving me multiple projects, almost every semester, for almost four years that were my own. You also gave me my first exposure to mentoring research students and teaching and I have continued with these in some capacity every year. When applying to my master's program you offered to take time off to visit departments of different schools if needed. When you went back to industry and I applied to PhD programs you again offered to visit various departments with me to help make sure I chose programs that were a good fit for me. I appreciate all that you have done and know that it has greatly shaped my career path.*

*To my parents, thank you for sticky by me for this long journey. I was not expecting to go for a masters or a PhD but you stuck by me no matter what I chose and remained supportive. I wish I could say I was finished with training for my career but I still have a lot more to do.*

# Acknowledgments

I would like to thank my committee members for volunteering their time, expertise, and use of facilities for the completion of my research. Thank you Dr. Yong W. Lee and Dr. Luke Achenie for serving as advisors and co-chairs for my committee and dedicating countless hours to each of my projects, even the ones that did not make it into this dissertation. Thank you Dr. Clay Gabler, Dr. Alexei Morozov, Dr. Aaron Goldstein, and Dr. John Rossmeisl for agreeing to serve on my committee.

Thank you to all of the people that not only helped prepare me for my doctoral program but also to the individuals that helped support me throughout it. I will only list a few here, but know that I remember everyone that supports me. A special thanks to Dr. Mark Van Dyke, Dr. Alexis Trent, Dr. Michele Waters, Dr. Jasmine Hayes, Dr. Jack Lesko, Dr. Catherine Amelink, Dr. Ed Smith, Dr. Menah Pratt-Clarke, Dr. Mercedes Ramírez Fernández, Marissa Lang, Demetrius Baskerville, and Deborah Smith.

I would like to acknowledge all of the sources of funding and support received over the course of this dissertation: Virginia Tech Initiative for Maximizing Student Development (VT-IMSD), College of Engineering New Horizon Graduate Scholars (COE-NHGS), the Graduate School, Dean of Students, College of Engineering, Biomedical Engineering and Mechanics (BEAM), School of Biomedical Engineering and Sciences (SBES), and Virginia Tech Center for Autism Research (VT-CAR).

I would also like to recognize all of the undergraduates that have assisted with these projects

at their various stages: Sean McLaughlin, Joshua James, Christopher Rasknick, Jihyeon 'Jane' Gong, Sukyoung 'Chloe' Kim, Vincent Sannicolas, Gina Muan, Sarah Woolverton, Molly Acord, Richard Yea, and Morgan Haywood.

# Contents

# List of Figures

# List of Tables

# List of Abbreviations

AD Alzheimer's disease

ASD Autism spectrum disorder

AUC Area under the curve

BBB Blood-brain barrier

BTBR BTBR T+ Itpr3tf/J

$C_{max}$ Max plasma concentration

C57 C57BL/6J

CL/F Clearance

CNS Central nervous system

CYP Cytochrome P450

$D_{eff}$ Effective diffusion constant

DHE Dihydroethidium

DMSO Dimethyl sulfoxide

FITC Fluorescein-5-isothiocyanate

HBMEC Human brain microvascular endothelial cell

I.P. Intraperitoneal

| | |
|---|---|
| MS | Multiple sclerosis |
| NaFl | Sodium fluorescein |
| PBS | Phosphate buffered saline |
| PK | Pharmacokinetic |
| ROS | Reactive oxygen species |
| $t_{1/2}$ | Terminal half-life |
| $t_{max}$ | Time to reach max plasma concentration |
| UGT | Uridine diphosphate glucuronosyltransferase |
| V/F | Apparent volume of distribution |
| XO | Xanthine oxidase |

# Chapter 1

# Introduction

## 1.1 Background

### 1.1.1 *Autism Spectrum Disorder and Economic Burden*

Autism spectrum disorder (ASD), also referred to as pervasive developmental disorder, is a lifelong neurodevelopmental disability that currently impacts as many as 1 in 59 children (Table 1.1) in the United States according to the 2014 surveillance data from the Autism and Developmental Disabilities Monitoring (ADDM) Network.[1] According to a study conducted by Christensen et al., ASD is reported to occur in males more than females at a ratio of 4.5: 1 (1 in 42 boys to 1 in 189 girls) and occurs in all racial, ethnic, and socioeconomic groups.[2] People with ASD have behavioral abnormalities in the areas of (1) social interaction, (2) verbal and non-verbal communication, and (3) restrictive and repetitive behaviors that can affect how they behave, learn, and interact with others.[3,4]

Currently, the route to diagnosis for children is through behavioral assessments and the Diagnostic and Statistical Manual (DSM) of Mental Disorders which has gone through multiple revisions (DSM-III to DSM-V) where now Asperger disorder (AD), pervasive developmental disorder-not otherwise specified (PDD-NOS), and autistic disorder all fall under the umbrella term ASD in the DSM-V. Concerns have been raised about people previously diagnosed with ASD under older editions of the DSM losing their diagnosis in later editions resulting in loss

Table 1.1: Reproduced from www.cdc.gov/ncbdd/autism/data.html for prevalence of ASD from ADDM Network Data.

| Surveillance Year | Birth Year | # ADDM Sites Reporting | Prevalence per 1,000 Children | Prevalence Range[a] | This is about 1 in X Children |
|---|---|---|---|---|---|
| 2000 | 1992 | 6 | 6.7 | 4.5 - 9.9 | 1 in 150 |
| 2002 | 1994 | 14 | 6.6 | 3.3 - 10.6 | 1 in 150 |
| 2004 | 1996 | 8 | 8.0 | 4.6 - 9.8 | 1 in 125 |
| 2006 | 1998 | 11 | 9.0 | 4.2 - 12.1 | 1 in 110 |
| 2008 | 2000 | 14 | 11.3 | 4.8 - 21.2 | 1 in 88 |
| 2010 | 2002 | 11 | 14.7 | 5.7 - 21.9 | 1 in 68 |
| 2012 | 2004 | 11 | 14.6 | 8.2 - 24.6 | 1 in 68 |
| 2014 | 2006 | 11 | 16.8 | 13.1 - 29.3 | 1 in 59 |

[a] per 1,000 children

of services. Studies comparing the DSM-IV to the DSM-V vary on levels of specificity and sensitivity depending on the assessment tools and cutoffs used. In a comprehensive study by Christiansz et al., looking at young children 2-17 years of age, it was found that high sensitivity (0.76-0.96) could be achieved but at the expense of specificity.[5,6]

In addition to these core deficits it is common to have co-occurrences (co-morbidity) of non-ASD diagnoses ranging from cognitive impairments, epilepsy, psychiatric illness, feeding disturbances, gastrointestinal illnesses, sleep disturbances, dysmorphism, and sensory abnormalities.[7–10]

The economic burden of childhood ASD on families is of a major concern as parents taking care of a child with ASD can expect to have high expenditures compared to parents taking care of children without an ASD. In a study conducted by Cidav et al. it was estimated that family earnings of children with ASD were 21% less than families of children with other health limitations and 28% lower than families of children without health limitations.[11] Lavelle et al. estimated the total societal burden of caring for individuals with ASD to be $11.5 billion in 2011 (about $17,081 per child) as parents reported higher health care and

non-health care costs and higher school costs.[12] In addition to the economic burden quality of care families receive is of importance as parents of children with ASD have reported difficulties with access to services and quality care by providers in the United States as there are a limited supply of pediatric specialists in that can provide care.[13] Home life can also be stressful as the demands of caring for a child with ASD has led to at least one parental caregiver leaving the workforce to provide necessary services and siblings of children with an ASD are at a high risk of negative psychological outcomes.[14,15]

### 1.1.2 *Autism Spectrum Disorder Causes and Intervention Routes*

The exact cause of ASD is not known but science suggests that there may be a multitude of causes such as (1) genetics,[16,17] (2) mitochondrial dysfunction,[18,19] (3) metabolic dysfunction,[20–22] (4) environmental,[23] and (5) oxidative stress.[24–27] With potential causes of ASD being multi-factorial and the occurrence of co-morbidities treatment/interventions would need to occur on multiple fronts including (1) behavioral interventions, (2) detoxification, (3) digestive, (4) nutritional supplementation, (5) immune function normalization, (6) pharmacological, and (7) reduction of oxidative stress (see Table 1.2).

Table 1.2: Summary of available resources for interventions for patients with ASD.

| Intervention Area | References |
|---|---|
| Behavioral (e.g. applied behavioral analysis) | [28,29] |
| Detoxification (e.g. chelation) | [30–32] |
| Digestive (e.g. restoration of gut flora) | [30,31] |
| Nutritional supplementation (e.g. vitamins) | [30–32] |
| Immune function | [30–32] |
| Pharmacological (e.g. mood stabilizers, anti-psychotics) | [33–35] |
| Reduction of oxidative stress (e.g. glutathione) | [30,36] |

There are various potential contributors to oxidative stress in the brain, in the case of

ischemic conditions lipid peroxidation, xanthine oxidase (XO), superoxide dismutases (SOD), catalase and glutathione peroxidase (GPx), glutathione, nitric oxide synthase, metals, poly (ADP-ribose) polymerase (PARP), mitochondrial permeability, and peroxynitrite have been implicated in pathways involved in brain damage.[37,38] Work conducted by Zoroglu et al. studied oxidative stress levels of erythrocytes of autistic children composed of 16 boys and 11 girls with an age range of 2-12 years with a mean age of 4.7 (± 2.7) years. Blood samples showed elevated levels of XO, thiobarbituric acid reactive substances (TBARS), and SOD in autistic patients compared to age matched controls.[39]

### 1.1.3 *Preliminary Research in Autism Mice*

Preliminary research conducted by the Lee lab group (Figure 1.1) compared the expression levels of oxidative stress-related genes in brain tissues of BTBR T+ Itpr3tf/J (BTBR) male mice to C57BL/6J (C57) male mice. Of the over 20+ mouse models of autism relevant behaviors, the BTBR mouse showed the most face validity to the diagnostic symptoms of autism: (1) reduced reciprocal social interactions, (2) low sociability, (3) increased repetitive self-grooming, (3) reduced social transmission of food preference, (4) abnormal ultrasonic vocalizations.[40] Three-week old male mice were used as ASD is diagnosed at a higher rate in males than females in the human population in children. While results showed elevated expression of XO in the autism model compared to controls, there were no significant differences in other markers of oxidative stress. Nevertheless, brain tissue fluorescent staining (Figure 1.2) of BTBR and C57 mice showed significantly higher levels of oxidative stress in BTBR mice compared to C57 mice using a dihydroethidium (DHE) stain.

As there are significantly elevated levels of XO in mouse brain tissue of BTBR mice compared to C57 controls and all other levels of oxidative stress were not significantly different between

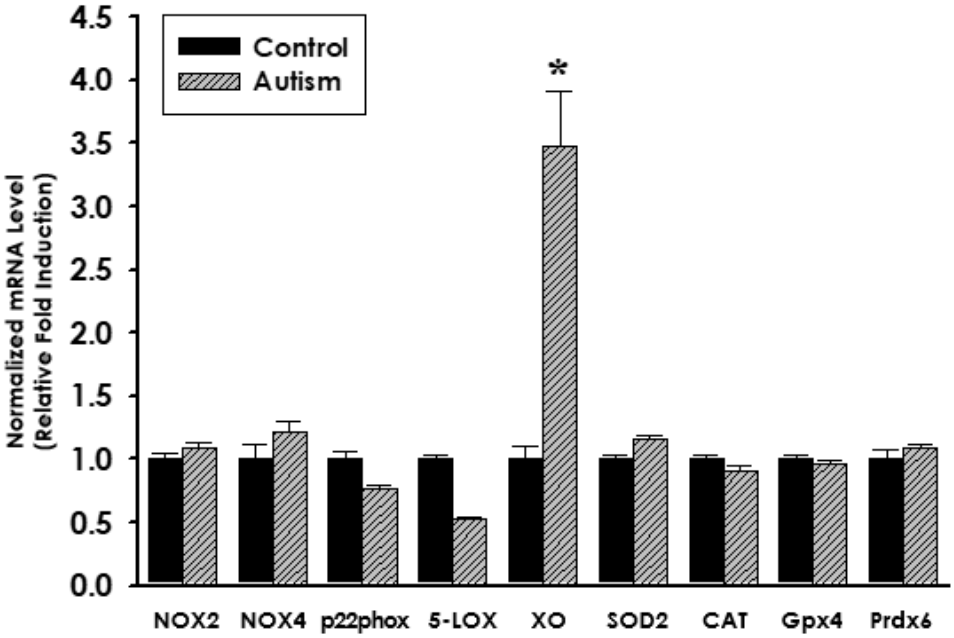


Figure 1.1: Comparison of mRNA levels of oxidative stress-related genes in the brains of 3 week old male BTBR mice compared to C57 mice. Xanthine oxidase expression in BTBR mice was significantly elevated compared to C57 mice ($p<0.05$). Unpublished data from work conducted by Lee lab group.

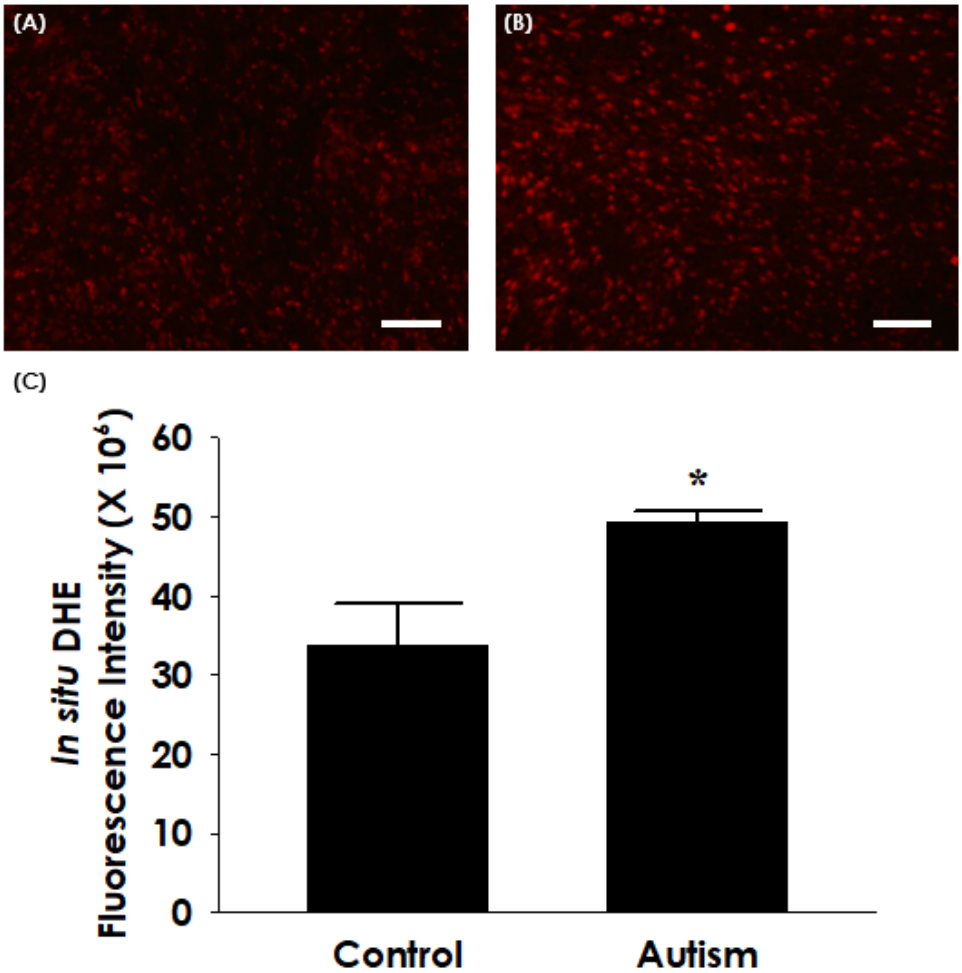


Figure 1.2: Comparison of oxidative stress levels in C57 (panel A) and BTBR (panel B) brain tissue using dihydroethidium (DHE) staining. Levels of oxidative stress in autism samples were significantly higher compared to C57 controls ($p<0.05$, $n=6$). Scale bar = 100 µm. Unpublished data from work conducted by Lee lab group.

groups, combined with the elevated level of oxidative stress found in brain tissue by DHE staining, it is hypothesized that XO plays a role in oxidative brain damage and that inhibition of XO can lead to the reduction in brain damage.

### 1.1.4 *Xanthine Oxidase and Inhibitors*

XO and xanthine dehydrogenase (XDH) are both forms of the enzyme xanthine oxidoreductase (XOR). The suggested mechanism of reactive oxygen species (ROS) generation involves XOR converting hypoxanthine to xanthine and xanthine to uric acid where both conversion steps release oxygen by-products that could lead to oxidative stress.[41–43] XOR is found to be distributed in plasma, brain, lungs, liver, small intestines, and kidneys of mammals with varying levels depending on the species[44–48] and has been found to be more than a marker of damage being implicated in tissue and organ damage as XO binds to endothelial cells and causes damage.[49]

The XO-inhibitor allopurinol has been around for decades as the primary compound of choice in inhibiting XO in gout. Allopurinol is an analogue of hypoxanthine with low lipid solubility (octanol: water partition coefficient of 0.28) that when converted to oxypurinol (octanol: water partition coefficient of 14) is responsible for most of the inhibiting effect on XO. Both allopurinol and oxypurinol are purine inhibitors (Figure 1.3) that can potentially interfere with purine metabolism of compounds other than hypoxanthine and xanthine. In addition to the non-selectivity of allopurinol, patients can experience hypersensitivity reactions (although rare).

Uloric (Febuxostat) is a newer compound that has higher potency than allopurinol and is a non-purine inhibitor with specificity for XO where it does not affect other purines.[50–52] In addition to generally being more potent than allopurinol, febuxostat has been shown

to be a more potent inhibitor of XO bound to endothelial cells at physiologic conditions (pH 7.4).[53] Once taken orally, febuxostat has a rapid intestinal absorption of around 84% with a half-life ranging from 1 – 18 hours depending on the dosage. While both febuxostat and allopurinol undergo hepatic metabolism, elimination by the kidneys is higher compared to that of allopurinol making it a suitable alternative for gout patients with renal impairment.[54,55] Additionally, the drug is highly bound to albumin in the blood (approximately 99%) and has a low to medium apparent volume distribution at steady state (0.7 L/kg). A comparison of properties (Table 1.3) using Drugbank (www.drugbank.ca) data shows that all three compounds were predicted to have the ability to cross the intestinal and blood-brain barrier (BBB) with higher predicted probabilities in allopurinol and oxypurinol compared to febuxostat. The solubility of febuxostat is greatly reduced (approximately 100x) compared to oxypurinol and allopurinol and it carries a negative charge. Allopurinol, which is used clinically over oxypurinol, has a shorter half life than febuxostat. With febuxostat having (1) higher potency, (2) higher inhibition of XO, (3) better selectivity of XO, and (4) a longer half life compared to allopurinol and oxypurinol this drug was chosen as a potential candidate to study its potential XO-inhibition capability in the brain tissue.

### 1.1.5 *Blood-Brain Barrier Physiology and Dysfunction in Disease*

One major obstacle of transport of febuxostat into the brain is the BBB which serves as a physical barrier between the brain and the blood to limit the passage of potentially harmful substances. The BBB is composed of endothelial cells connected by tight junctions (TJs) and adherens junctions (AJs) that are partially responsible for the BBB's selective nature. The main mechanisms allowing the transport of drugs across are (1) passive diffusion, (2) carrier-mediated transport, (3) receptor-mediated transcytosis, and (4)

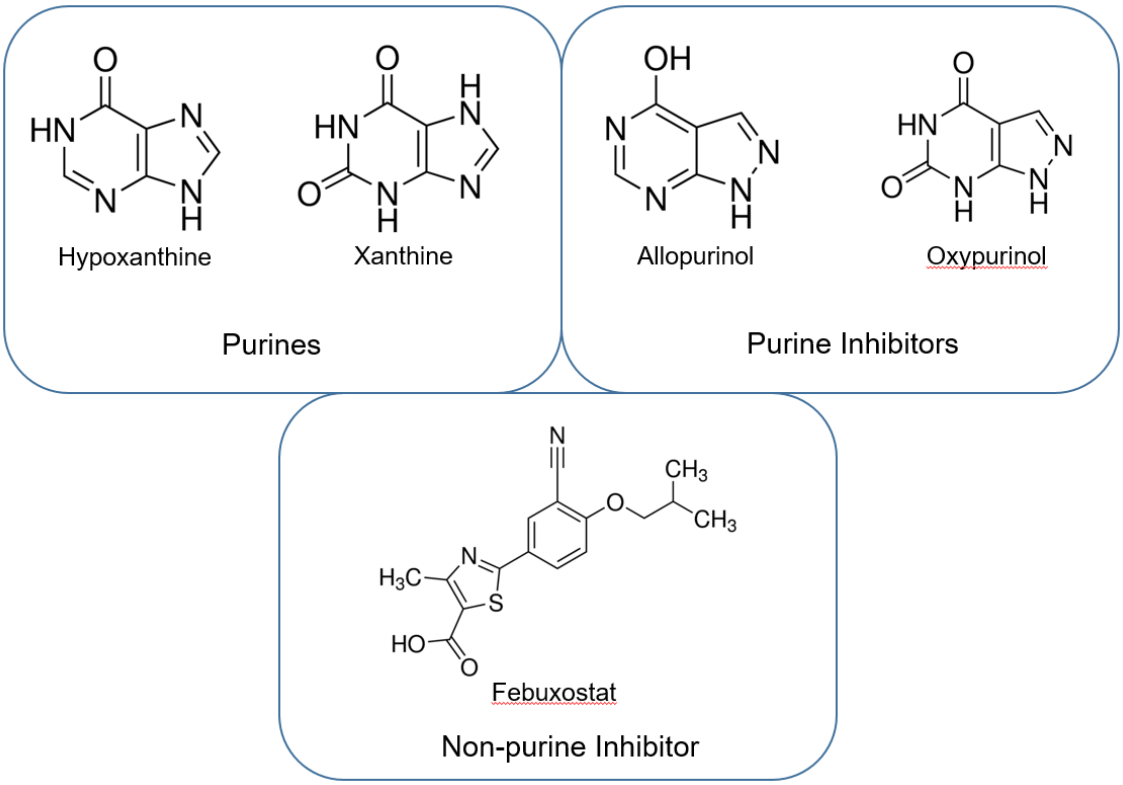


Figure 1.3: Chemical structures (Sigma-Aldrich) of hypoxanthine, xanthine, allopurinol, oxypurinol, and febuxostat.

Table 1.3: Pharmacology, predicted properties, and predicted absorption, distribution, metabolism, excretion, and toxicity (ADMET) properties of allopurinol, oxypurinol, and febuxostat.

| Name | Allopurinol | Oxypurinol | Febuxostat |
|---|---|---|---|
| Molecular Weight | 136.11 | 152.11 | 316.375 |
| Water Solubility (mg/mL) | 5.88 | 2.32 | 0.0183 |
| Half Life (hrs) | 1 - 3 | 23.3 (+/- 6hrs) | 5 - 8 |
| Physiologic Charge | 0 | 0 | 0 |
| Human Intestinal Absorption | Value = (+)<br>Prob = 0.997 | Value = (+)<br>Prob = 1.0 | Value = (+)<br>Prob = 0.9865 |
| Blood-Brain Barrier (BBB) | Value = (+)<br>Prob = 0.9885 | Value = (+)<br>Prob = 0.9947 | Value = (+)<br>Prob = 0.7853 |
| Caco-2 Permeable | Value = (+)<br>Prob = 0.6232 | Value = (-)<br>Prob = 0.6863 | Value = (+)<br>Prob = 0.5126 |

adsorption-mediated transcytosis.[56–58] In a diseased state, where neuro-inflammation and oxidative stress are elevated, increased BBB breakdown and dysfunction can occur which has been documented in encephalitis,[59,60] multiple sclerosis (MS),[59–65] stroke[59–62,66] or brain trauma,[59,61] hypertension,[60] tumors,[60] amyotrophic lateral sclerosis (ALS),[61,62] Alzheimer's disease (AD),[61,63,64,67] and ASD.[68] Under this state drugs that previously were unable to cross the BBB have a higher potential of crossing from the blood once absorbed from the gastrointestinal tract.

### 1.1.6 *Drug Transport and Metabolism: Cytochrome P450 and Uridine Diphosphate Glucuronosyltransferases*

The oral absorption and metabolism of drug substances by the body is a multi-phase process where drugs broken down and dissolved by the stomach begin their transit into the proximal small intestine (duodenum) followed by transit through the jejunum and ileum of the small intestine and finally into the large intestine. It is in the small intestine that a majority of absorption occurs where drug substances are transported to the portal vein and then on to the systemic circulation. Along this route drugs undergo phase I (oxidation, reduction, and hydrolysis) and phase II (glucoronidation) metabolism in both the gut and liver[69,70]. Cytochrome P450 (CYP) enzymes oxidize xenobiotic (foreign) substances and can be found on the mitochondria and smooth endoplasmic reticulum (ER) of epithelial cells of the small intestine and hepatocytes. Outside of the gut and liver the brain also has the capacity to metabolize drugs through CYP enzymes, although this capacity is reduced compared to the liver and has been estimated to range from 0.5-2% and up to 10% of that found in the liver.[71,72] Uridine diphosphate (UDP) glucuronosyltransferases (UGTs) are a family of enzymes found in tissues such as the brain, skin, spleen, prostate, gastrointestinal tract, lung, and kidneys but the liver is the main site of glucuronidation for phase II metabolism.[73]

Although drugs can be designed to target various areas in the body consideration must still be given to unintended areas in the body in both healthy and diseased states so that patient safety can be maintained if drugs are metabolized in other tissues. Computational approaches involving pharmacokinetics can be used to help understand what the body does to a drug following various administration routes into different tissues such as the brain.

### 1.1.7 *Pharmacokinetic Modeling of Febuxostat to the Central Nervous System*

Pharmacokinetics (PK) can be used to study the absorption, distribution, metabolism, and excretion of drug compounds based on clinical data. Multi-compartment modeling makes use of the PK data by tracking the concentrations and levels of the drug compound and its metabolites over time (concentration vs. time curves). These types of models can be important tools with potential uses in individualized patient care of dose regimens, improvements in drug formulations, and used as predictive models to simulate longer time scales of drug regimens in patients.[74]

Human PK data was collected from a search of databases and clinical trials (clinicaltrials.gov) that listed results for single dose and multiple dose studies (Table 1.4) of oral drug administration of febuxostat in blood plasma. Parameters such as (1) time to reach max plasma concentrations $t_{max}$, (2) max plasma concentration $C_{max}$, (3) area under the plasma concentration curve (AUC) from zero to the last measurable concentration ($AUC_t$), (4) terminal half-life ($t_{1/2}$) of the drug, (5) clearance (CL/F), and (6) apparent volume of distribution (V/F) were compared between multiple studies. PK data in humans beyond the plasma compartment is difficult to obtain as it would require sampling of living human subjects from multiple organ and tissue sites which adds to the difficulty of creating a PK model

with useful predictive capabilities.

Table 1.4: Human plasma pharmacokinetic (PK) studies for febuxostat. Caucasian (W), Black (B), Asian (A), Hispanic (H).

| Age | Race | Gender | Dose (mg) Single | Dose (mg) Multiple | References |
|---|---|---|---|---|---|
| 18-55 | W/H/B/A | M/F | 40,120 | 80 | [75] |
| 18-40 | A | M | 40,80 | - | [76] |
| 18-65+ | A | M/F | 10-240 | 10-240 | [77] |
| 22-74 | - | - | - | 20 | [78] |
| 18-40 | A | M/F | 40,80,120 | 80 | [79] |
| 39-62 | W/H/B | M/F | - | 80 | [80] |
| 19-54 | - | M/F | 40-120 | 40-120 | [81] |
| 36-69 | W/H/B/A | M/F | - | 80 | [82] |
| 21-47 | W/H/B/A | M/F | 10-240 | 10-240 | [83] |
| 18-40 | A | M/F | 40,80,120 | - | [84] |
| - | - | - | 40,80,120 | - | [85] |
| 20-45 | - | M | 80 | - | [86] |

Due to the lipophilicity of febuxostat it has the potential to cross lipid bilayers by passive diffusion making it potential candidate to cross the BBB to inhibit XO. With the high binding affinity of febuxostat to albumin, only a low amount of free drug remains unbound to cross the BBB. The rates of association and dissociation of drug from albumin are important considerations to determine the potential amounts of febuxostat that can enter the CNS and penetrate into the brain tissue.[87–89]

### 1.1.8 *Specific Aims and Significance*

The specific aims of the project are to (1) model transport lipophilic compounds across a blood-brain barrier mimic, (2) determine if XO-inhibition lowers oxidative stress resulting in cognitive improvement, and (3) create a pharmacokinetic multi-compartment model to study the distribution and penetration of febuxostat into the central nervous system and

brain tissue.

The overall significance of this work is that it begins to study the potential transport, distribution, and behavioral improvements of autistic behaviors in an autism mouse model with XO-inhibition. As the current mechanism of febuxostat transport into brain tissue is unknown and there are no models exploring the drugs transport and distribution, this work will help make a significant contribution to future pharmacokinetic models. If the proposed link between XO-induced brain damage and behavior is validated with improvements brought on by febuxostat treatment, our computational models will have uses in both animal and clinical research settings. The computational models created will allow researchers to simulate various dosing schemes to create individualized patient specific treatment plans.

### 1.1.9 *Innovation*

The approach to use fluorescent compounds, under specific aim 1, with properties close to febuxostat in a short-term *in vitro* set-up is unique in that it allows us to back out modeling parameters which could then be used to simulate longer scenarios. Overall, this approach is inexpensive and can make use of small sample amounts to determine the amount of uptake into cell monolayers. The approach taken under specific aim 2 focuses on directly targeting the XO enzyme to reduce oxidative stress to reduce brain damage instead of targeting receptors at the BBB in hopes of improving behavioral outcomes. To our knowledge, there have been no single pharmacokinetic multi-compartment models looking at CNS single dosing schedules of febuxostat in humans. The innovation of specific aim 3 yields a model that can be used in simulations to predict potential dosing amounts and dosing schedules of patients to reach an optimum level of unbound febuxostat to penetrate into brain tissue. The human model can also be scaled down to rodent models to help in dosing schemes.

# Chapter 2

# A Passive Diffusion Model of Fluorescein Derivatives in an *In Vitro* Human Brain Microvascular Endothelial Cell (HBMEC) Monolayer

**Jamelle M. Simmons, Luke Achenie, Yong W. Lee**

**Published in Journal of Measurement Engineering**

Eukaryotic cells have a protective plasma membrane, which restricts the free movement of molecules from the external environment to the internal environment. This study aims to computationally model the transport of fluorescein derivatives across the monolayer of human brain microvascular endothelial cells (HBMEC). The determination of plausible effective diffusion constants ($D_{eff}$) will allow models to be built that could be useful beyond *in vitro* experimentation. Fluorescein-5-isothiocyanate (FITC) modeling produced a $D_{eff}$ range of 1E-20 to 5E-20 $cm^2/s$ at a 1 µm cell monolayer thickness and a $D_{eff}$ constant near 5E-29 $cm^2/s$ at a 5 µm cell monolayer thickness. Both fluorescein and sodium fluorescein (NaFl)

modeling at the 1 and 5 µm thicknesses did not produce simulations that closely resembled the HBMEC *in vitro* model. Overall, it is possible that the fluorescent intensity noted with fluorescein and NaFl may be better explained by a mechanism other than passive diffusion. Simulations of FITC diffusion produced a narrow range of $D_{eff}$ constants that closely matched the *in vitro* HBMEC fluorescent intensity.

## 2.1 Introduction

Eukaryotic cells are enclosed in a plasma membrane which separates the external and internal environments that serves as protection for the cells. The lipid bilayer of the plasma membrane is composed of hydrophilic head groups which are directed towards the aqueous exterior and interior portions of cells and hydrophobic tails separating the hydrophilic groups. The plasma membrane is mostly composed of lipids and proteins that help it form a barrier around the cell's internal environment.[90–92]

Isothiocyanates (ITCs) are small molecules found in vegetables that are capable of binding to amino groups and proteins and passively diffuse through gastrointestinal epithelium and capillary endothelium.[93,94] Phenethyl isothiocyanate (PEITC) has been shown to be absorbed into human non-small lung carcinoma (A549) cells and ITCs bind to thiol groups at a faster rate compared to amino groups under basic conditions.[95–98] Research on the cellular accumulation of ITCs has found that the uptake is dependent on intracellular levels of glutathione (GSH) and not dependent on the lipophilicity.[99–101]

Fluorescein-5-isothiocyanate (FITC, Isomer I) is a fluorescein fluorochrome conjugated to an isothiocyanate (ITC) that covalently binds to proteins and amine groups. When the pH is raised to an alkaline environment, the covalent bonding is stronger than at physiologic pH.[102–104] FITC has been shown to incorporate into the lipid layer and bind to membrane proteins of baby hamster kidney fibroblast (BHK) cells[105,106] and has been shown to label B and T lymphocytes differently as well bind to internal components of these cells.[107,108] Labeling of cells using FITC has been shown to be more uniform compared to other lipophilic labels such as 1,1'-dioctadecyl-3,3,3',3'-tetramethylindocarbocyanine perchlorate (Dil), but the FITC fluorescence decreases more rapidly compared to labels using tetramethylrhodamine (TRITC) under incubation at 37°C.[109] Additional factors that influence the flu-

orescence of cells are (A) concentration of fluorescent compound, (B) pH, (C) incubation time, (D) temperature, (E) concentration of cells, and (F) concentration of protein in cell culture medium.[107]

Sodium fluorescein (NaFl) is a water-soluble dye that has been used to evaluate the permeability of blood-brain barrier (BBB) models[110] due to its small size. It has also been used in the study of malignant and normal cells for its internal accumulation due to a pH gradient across the external and internal cell environments.[111] Fluorescein has high binding affinity to intracellular proteins of cells after it is hydrolyzed from a starting material, such as fluorescein diacetate (FDA), which is able to be taken into cells[112,113] but free diffusion of fluorescein has yet to be proven to our knowledge.

To date, many studies have been conducted on multiple cell types to determine the amount of cell surface attachment and cytoplasmic staining but work has not been done to determine if fluorescent tracers such as FITC, fluorescein, and NaFl can passively diffuse through the cell surface of human brain microvascular endothelial cells (HBMEC). Brain microvascular endothelial cells help make up the BBB which limits passage across it, to (1) active and passive transport, (2) endocytosis, (3) active and passive diffusion, and (4) paracellular transport, due to tight junctions between endothelial cells. Passive diffusion across cells remains a challenge as it is limited by lipophilicity, size, and charge of the cell and the compound diffusing across it.[114,115]

Additional parameters of interest, cell volume and size fluctuations, of cell monolayers can occur over time that will make an in vitro model more of a dynamic system. Studies conducted on Mandin-Darby canine kidney (MDCK) cells have volume fluctuations of $\pm 20\%$ and an average cell thickness of $7.1 \pm 0.7\,\mu\text{m}$ (mean $\pm$ standard deviation).[116] Confocal fluorescence microscopy has also been used to measure the cell thickness of C3H10T1/2 and V79 cells grown on various substrates. It was reported that C3H10T1/2 cells, during the

exponential growth phase, grown on mylar have an average cell thickness of 2.9 ± 0.6 µm while V79 cells have an average cell thickness of 6.1 ± 1.0 µm grown on the same substrate during the exponential growth phase.[117]

The aim of the present study was to create a simple approach that relies on fluorescence to determine an effective diffusion constant ($D_{eff}$) of FITC, fluorescein, and NaFl transport across human brain microvascular endothelial cells (HBMEC) by passive diffusion. These constants would allow simulations to be run which could help predict the amount of free diffusion into HBMEC monolayers overtime without loss of fluorescent intensity in signal that can be seen with prolonged in vitro incubation.

## 2.2 Materials and Methods

### 2.2.1 *Cell Culture*

Penicillin-streptomycin solution (100x), MEM vitamin solution (100x), endothelial cell growth supplement (ECGS), fetal bovine serum (FBS), and NuSerum culture supplement were all obtained from Corning Life Sciences. Sodium pyruvate solution (100mM), RPMI 1640 medium containing 2mM L-glutamine were purchased from GE Healthcare Life Sciences. Non-essential amino acids were obtained from Gibco laboratories. Human brain microvascular endothelial cells (HBMEC) were isolated and purified as previously described.[118] Cells were cultured in RPMI 1640 medium with 10% fetal bovine serum, 10% NuSerum, 30 µg/mL ECGS, 15 U/mL of heparin, 11.0 mg/mL of sodium pyruvate, 100 U/mL of penicillin, 100 µg/mL of streptomycin, nonessential amino acids, and vitamins. HBMEC cultures were incubated at 37°C in a humid environment with 5% $CO_2$.

### 2.2.2 *In Vitro Studies*

Fluorescein isothiocyante isomer I (FITC), fluorescein free acid, and fluorescein sodium salt (NaFl) fluorescent tracers were all purchased through Sigma-Aldrich. The molecular weights for FITC, fluorescein, and NaFl were 389.38, 332.31, and 376.28 respectively. HBMEC were grown to confluence followed by washing the monolayer with Hanks' balanced salt solution (HBSS, Corning Life Sciences) and cell detachment with 0.05% trypsin containing EDTA (GE Healthcare Life Sciences). The suspended cells were seeded into Falcon$^{TM}$48 well plates at a density of 7.0 x $10^4$ cells per well and grown to confluence in an incubator for 1-2 days.

Confluent cells were aspirated of media and replaced with 200 µL of 0.1 mg/mL fluorescent tracer solutions in basal RPMI 1640 medium. Wells were incubated in tracer solutions at 3, 6, 9, 12, 15, 18, 21, and 24 hours with a sample size of 6 wells per time point for all three tracers. All wells were washed twice with sterile phosphate buffered saline (1x) to remove excess fluorescent tracer and replaced with phenol free RPMI 1640 medium (Gibco Laboratories) at a volume of 200 µL. Fluorescent intensity of the wells were recorded using a SpectraMax $M2^e$ (Molecular Devices, LLC) plate reader with excitation and emission settings of 492 and 518 nm respectively for FITC, 490 and 514nm for fluorescein, and 460 and 515 nm for NaFl.

The fluorescent intensity was correlated to concentration (mg/mL) using a dilution curve generated for each fluorescent tracer dissolved in phenol red-free RPMI 1640 for various known concentrations. The fluorescent intensity of tracer found in the HBMEC monolayers were converted to concentration using the dilution curves. The total mass in mg for each monolayer was determined by multiplying the volume the monolayer occupied in each well by the calculated concentration. As cell monolayer thicknesses can vary based on cell type a 1 µm and 5 µm thickness were assumed within each well. The 48 well plates have a growth

area of 0.75 $cm^2$ and accounting for a 1 µm monolayer thickness results in a volume of 2.36E-04 mL being occupied by the monolayer while a 5 µm thickness results in a volume of 1.18E-03 mL being occupied by the monolayer. The total mass in mg was averaged and standard deviation calculated for each time point for each tracer (Figure 2.1).

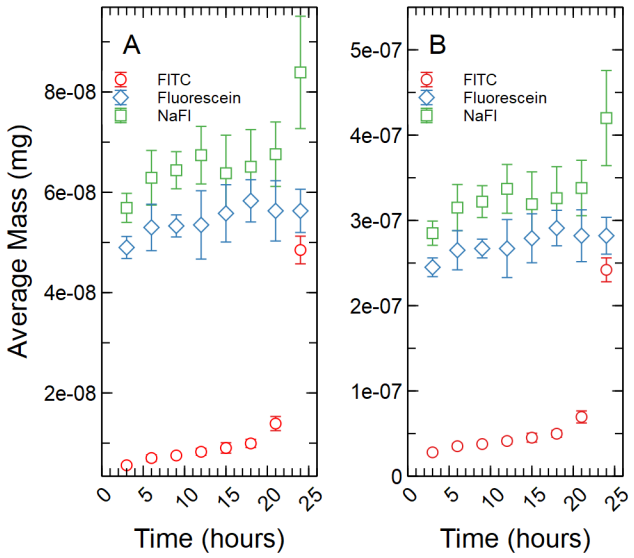


Figure 2.1: (A) Total mass in mg averaged for each time point per fluorescent tracer for a 1 µm thickness. (B) Total mass in mg averaged for each time point per fluorescent tracer for a 5 µm thickness.

### 2.2.3 *Passive Diffusion Model*

The in vitro system was composed of a cylindrical well where uptake of tracer could occur in the x, y, and z-directions (Figure 2.2) with the HBMEC. Assuming the transport mechanism is primarily through passive diffusion, the following simplifications were made: (1) no reaction terms, (2) no binding, (3) movement of tracer was uniform in all directions, and (4) an overall diffusion constant is appropriate. These assumptions allow for the reduction of the problem from a three dimensional (3D) space to a one dimensional (1D) space where concentration could be determined in the z-direction. A 1D partial differential equation (PDE,

equation(2.1)) was generated with one initial condition (equation (2.2)) and two boundary conditions (equations (2.3) and (2.4)). Simulations were run in MATLAB 2015b.

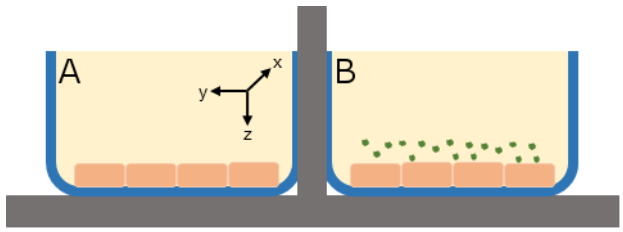


Figure 2.2: (A) *In vitro* cell culture of HBMEC where the monolayer thickness spans the z-direction. (B) Introduction of fluorescent tracers to the HBMEC for incubation. Uptake of the tracer is assumed to be uniform in all directions.

$$\frac{\partial c}{\partial t} = \frac{\partial}{\partial z}(D_{eff}\frac{\partial c}{\partial z}) \tag{2.1}$$

$$c(0, z) = 0,\ at\ t = 0\ for\ all\ z \tag{2.2}$$

$$c(t, 0) = 0.1mg/mL,\ at\ surface\ (z = 0)\ for\ t > 0 \tag{2.3}$$

$$\frac{\partial C}{\partial t} = 0,\ at\ bottom\ (z = L)\ for\ t \geq 0 \tag{2.4}$$

The boundary concentration was set at 0.1 mg/mL for all simulations with the monolayer thickness varying between 1 µm and 5 µm which resulted in a monolayer volume of 2.36E-04 and 1.18E-03 mL respectively. A tracer concentration of 0.1 mg/mL was chosen for simulations to match the concentration used in the *in vitro* set-up. The monolayer thickness in the z-direction was divided into 70 evenly spaced pieces for simulations and the time span was restricted to 24 hours. A range of effective diffusion constants were simulated where the resulting concentration (mass/volume) was converted to mass in mg and the area under the curve for each time point was generated for comparison with the HBMEC *in vitro* data.

The *in vitro* data was split into a calibration and validation group where time points at hours 3, 12, 15, 21, and 24 were allocated to the calibration set and time points at hours 6, 9, and 18 were allocated to the validation set. A range of effective diffusion constants ($D_{eff}$, $cm^2/s$) were selected for simulations and simulated time points at hours 3, 12, 15, 21, and 24 were extracted and compared to the *in vitro* time points at those hours to determine a range of diffusion constants that produced results not statistically significantly different from the *in vitro* data. The resulting diffusion constants were used to run simulations and extract time points at hours 6, 9, and 18 and those were compared to the *in vitro* time points at those hours. The percent error was calculated for the validation sets to determine how far the simulated models deviated from the *in vitro* model.

### 2.2.4 *Statistical Methods*

The means of each experimental time point for each fluorescent tracer were compared using an Analysis of Variance (ANOVA) if equal variance could be assumed at all time points per tracer otherwise the non-parametric equivalent of an ANOVA (Welch Test) was used. Post-hoc comparisons were conducted if the p-value of the ANOVA was less than the alpha ($p<0.05$). The Games-Howell post-hoc test was used if the non-parametric ANOVA was conducted and a Tukey Honest Significant Differences (HSD) was used if the parametric ANOVA was conducted.

A linear regression comparison of slopes was used to compare the in vitro time points to the simulated time points for the calibration data at hours 3, 12, 15, 18, 21, and 24. A p-value less than 0.05 indicates the slopes of the in vitro and simulated models are significantly different while a p-value larger than 0.05 indicates the slopes are not statistically significantly different. All statistical testing was conducted using Minitab 18 software (Minitab, Inc). Plots were

generated using Veusz software.

## 2.3 Results

### 2.3.1 *In Vitro Diffusion of Fluorescent Tracers*

With the assumption of a 1 µm monolayer thickness, the calculated total average mass (mg) of tracer for FITC increased from 5.59E-09 mg with a standard deviation of 3.85E-10 mg after 3 hours of incubation to 4.85E-08 ± 2.76E-09 mg at 24 hours (Figure 2.1A). A non-parametric Welch Test was used to compare average mass among all FITC time points at the 95% confidence level resulting in an F-statistic = 192.36 and a p-value of 0.00. A Games-Howell post-hoc multiple comparison test was used showing the 24 and 21 hour time points to be significantly greater than all earlier time points (p-value $< 0.05$). The 18 hour time point was significantly greater than the 3 through 12 hour time points (p-value $< 0.05$). The 15 hour time points were significantly greater than the 3 and 6 hour time points (p-value $< 0.05$). The 12, 9, and 6 hour time points were significantly greater than the 3 hour time point with p-values of 0.001, 0.00, and 0.022 respectively. Fluorescein contents increased from 4.90E-08 ± 1.94E-09 mg at 3 hours to 5.63E-08 ± 4.31E-09 mg at 24 hours of incubation (Figure 2.1A). An ANOVA was used to compare all time points among the fluorescein data set resulting in an F-statistic = 2.19 and a p-value = 0.056, no additional post-hoc statistical testing was conducted. NaFl contents increased from 5.69E-08 ± 2.90E-09 mg at 3 hours to 8.39E-08 ± 1.12E-08 mg at 24 hours of incubation (Figure 2.1A). A non-parametric Welch Test was conducted resulting in an F-statistic = 6.33 and a p-value = 0.001. A Games-Howell post-hoc test showed only the 24 hour time point being significantly greater than the 3 and 6 hour time points with p-values of 0.016 and 0.046 respectively. The

9 hour time point was significantly greater than the 3 hour time point with a p-value of 0.045.

Under the assumption of a 5 µm monolayer thickness, the calculated total average mass in mg of tracer for FITC increased from 2.80E-08 mg with a standard deviation of 1.94E-10 mg after 3 hours of incubation to 2.42E-07 ± 1.40E-08 mg at 24 hours (Figure 2.1B). Fluorescein contents increased from 2.45E-07 ± 1.10E-08 mg at 3 hours to 2.82E-07 ± 2.16E-08 mg at 24 hours of incubation (Figure 2.1B). NaFl contents increased from 2.85E-07 ± 1.42E-08 mg at 3 hours to 4.20E-07 ± 5.58E-08 mg at 24 hours of incubation (Figure 2.1B). The statistical testing at the 5 µm monolayer thickness returned the same results as those found above with the 1 µm monolayer thickness.

### 2.3.2 *Linear Regression: FITC Calibration*

For a 1 µm monolayer thickness, FITC calibration simulations run using effective diffusion constants ($D_{eff}$) of 5.00E-21, 1.00E-20, and 5.00E-20 $cm^2/s$ (Figure 2.3A) created a range of data close to the in vitro calibration data set at hours 3, 12, 15, 18, 21, and 24 hours. The slopes of each simulated data set were statistically compared to the *in vitro* data set using a linear regression approach. There was not a significant difference in slopes comparing the 5.00E-21 $cm^2/s$ simulation to the *in vitro* data set with a t-statistic of 2.179 and a p-value of 0.066. The 1.00E-20 and 5.00E-20 $cm^2/s$ simulations yielded similar results with t-statistics of 2.011 and 0.314 respectively with p-values of 0.084 and 0.763 respectively.

With a 5 µm monolayer thickness, calibration simulations run using effective diffusion constants ($D_{eff}$) of 5.00E-21 and 1.00E-20 $cm^2/s$ (Figure 2.3B) resulted in t-statistics of 1.647 and 4.865 respectively with p-values of 0.144 and 0.002 respectively when compared to *in vitro* data.

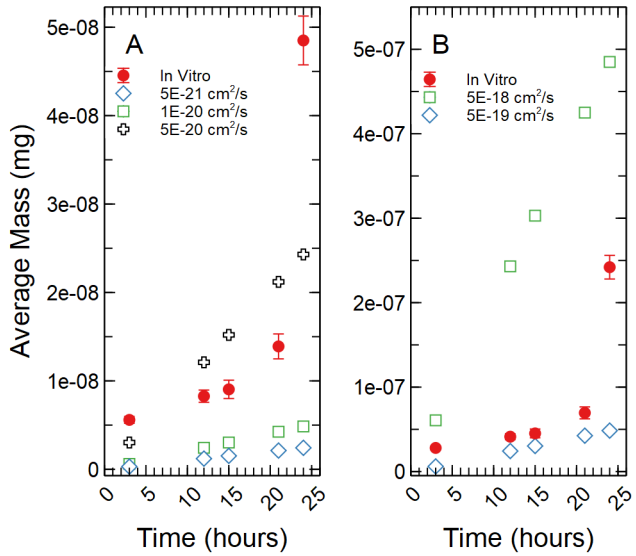


Figure 2.3: (A) Simulations run under a 1 µm monolayer thickness assumption, all simulations were found to not be statistically significantly different from the in vitro data. (B) Simulations run under a 5 µm monolayer thickness assumption, using a simulated $D_{eff}$ of 5.00E-21 cm$^2$/s was shown to not be statistically significant while a simulated $D_{eff}$ of 1.00E-20 cm$^2$/s yielded a significant difference at a p-value of 0.002 for FITC.

### 2.3.3 *Linear Regression: Fluorescein Calibration*

For a 1 µm monolayer thickness, fluorescein calibration simulations run using effective diffusion constants ($D_{eff}$) of 5.00E-21 and 1.00E-20 cm$^2$/s (Figure 2.4A) created a range of data close to the *in vitro* calibration data set at hours 3, 12, 15, 18, 21, and 24 hours. The slopes of each simulated data set were statistically compared to the *in vitro* data set using a linear regression approach. There was a significant difference in slopes comparing the 5.00E-21 and 1.00E-20 cm$^2$/s simulations to the *in vitro* data set with t-statistic of 5.122 and 3.594 respectively and p-values of 0.001 and 0.009 respectively.

With a 5 µm monolayer thickness, calibration simulations run using effective diffusion constants ($D_{eff}$) of 1.00E-18, 5.00E-18, and 1.00E-17 cm$^2$/s (Figure 2.4B) resulted in t-statistics of 31.364, 0.632, and 3.125 respectively and p-values of 8.65E-9, 0.547, and 0.017 respectively.

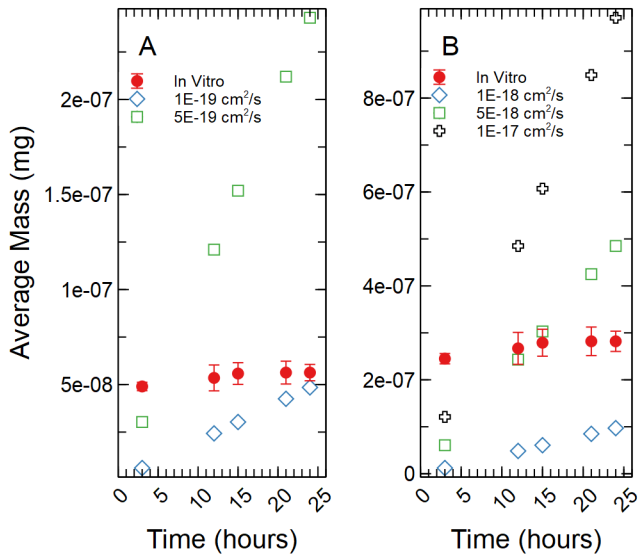


Figure 2.4: (A) Simulations run under a 1 µm monolayer thickness assumption, all simulations were found to be statistically significantly different from the *in vitro* data with p-values $< 0.05$. (B) Simulations run under a 5 µm monolayer thickness assumption were found to be statistically significant (p-value $< 0.05$) for both the 1.00E-18 and 1.00E-17 $cm^2/s$ effective diffusion constants with the 5.00E-18 $cm^2/s$ diffusion constant gave a p-value of 0.547.

### 2.3.4 *Linear Regression: NaFl Calibration*

For a 1 µm monolayer thickness, fluorescein calibration simulations run using effective diffusion constants ($D_{eff}$) of 5.00E-20 and 5.00E-19 $cm^2/s$ (Figure 2.5A) created a range of data close to the *in vitro* calibration data set at hours 3, 12, 15, 18, 21, and 24 hours. The slopes of each simulated data set were statistically compared to the *in vitro* data set using a linear regression approach. There was a significant difference in slopes comparing the 5.00E-20 and 5.00E-19 $cm^2/s$ simulations to the in vitro data set with t-statistic of 20.793 and 3.297 respectively and p-values of 1.49E-07 and 0.013 respectively.

With a 5 µm monolayer thickness, calibration simulations run using effective diffusion constants ($D_{eff}$) of 5.00E-19, 5.00E-18, and 5.00E-17 $cm^2/s$ (Figure 2.5B) resulted in t-statistics of 20.131, 0.831, and 4.923 respectively and p-values of 1.87E-07, 0.433, and 0.002 respectively.

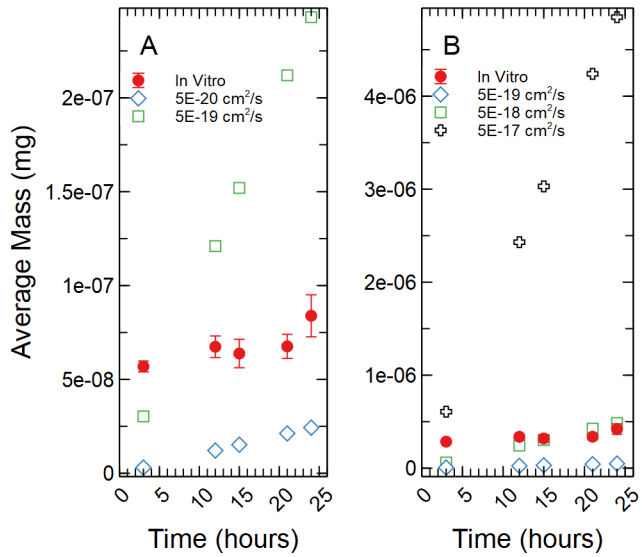


Figure 2.5: (A) Simulations run under a 1 µm monolayer thickness assumption, all simulations were found to be statistically significantly different from the *in vitro* data with p-values $< 0.05$. (B) Simulations run under a 5 µm monolayer thickness assumption were found to be statistically significant (p-value $< 0.05$) for both the 5.00E-19 and 5.00E-17 $cm^2/s$ effective diffusion constants with the 5.00E-18 $cm^2/s$ diffusion constant gave a p-value of 0.547.

### 2.3.5 *Percent Error: FITC, Fluorescein, NaFl Validation*

When increasing the effective diffusion ($D_{eff}$) constant of FITC, under a 1 µm assumption from 1E-20 to 5E-20 $cm^2/s$ shows a reduction in percent error of prediction of simulations (Table 2.1) at time points of 6 and 9 hours, but an increase in percent error of prediction at 18 hours of the validation data set using equation (2.5). When the monolayer thickness is increased to 5 µm and the $D_{eff}$ range is 5.00E-19 and 5E-18 $cm^2/s$ the percent error of prediction increased for all time points (Table 2.2).

$$\%Error = \frac{Simulation - In\ vitro}{In\ vitro} \times 100 \tag{2.5}$$

For fluorescein, under a 1 µm assumption, the $D_{eff}$ from 1E-19 to 5E-19 $cm^2/s$ shows a reduction in percent error of prediction of simulations (Table 2.3) at the 6 hour time point

Table 2.1: FITC simulated mass (mg) compared to average *in vitro* mass. Monolayer thickness of 1 µm, volume of 2.36E-04 mL. All mass multiplied by 1E-09.

| Time (hrs) | *In Vitro* (mg) | $D_{eff}$[a] (mg) | % error | $D_{eff}$[b] (mg) | % error |
|---|---|---|---|---|---|
| 6 | 7.03 | 1.21 | 82.74 | 6.07 | 13.69 |
| 9 | 7.54 | 1.82 | 75.86 | 9.10 | 20.68 |
| 18 | 9.94 | 3.64 | 63.38 | 18.2 | 83.09 |

[a] $D_{eff}$ =1E-20 $cm^2/s$
[b] $D_{eff}$ =5E-20 $cm^2/s$

Table 2.2: FITC simulated mass (mg) compared to average *in vitro* mass. Monolayer thickness of 5 µm, volume of 1.18E-03 mL. All mass multiplied by 1E-08.

| Time (hrs) | *In Vitro* (mg) | $D_{eff}$[a] (mg) | % error | $D_{eff}$[b] (mg) | % error |
|---|---|---|---|---|---|
| 6 | 3.52 | 1.21 | 65.48 | 12.1 | 245.23 |
| 9 | 3.77 | 1.82 | 51.72 | 18.2 | 382.82 |
| 18 | 4.98 | 3.64 | 26.85 | 36.4 | 631.50 |

[a] $D_{eff}$ =1E-19 $cm^2/s$
[b] $D_{eff}$ =5E-18 $cm^2/s$

and an increase in error rate at the 9 and 18 hour time points (Table 2.3). Under a monolayer assumption of 5 µm there is a reduction in percent error at all three time points (Table 2.4).

Table 2.3: Fluorescein simulated mass (mg) compared to average *in vitro* mass. Monolayer thickness of 1 µm, volume of 2.36E-04 mL. All mass multiplied by 1E-08.

| Time (hrs) | *In Vitro* (mg) | $D_{eff}$[a] (mg) | % error | $D_{eff}$[b] (mg) | % error |
|---|---|---|---|---|---|
| 6 | 5.30 | 1.21 | 77.12 | 6.07 | 14.41 |
| 9 | 5.33 | 1.82 | 65.85 | 9.10 | 70.75 |
| 18 | 5.83 | 3.64 | 37.50 | 18.2 | 212.47 |

[a] $D_{eff}$ =1E-19 cm$^2$/s
[b] $D_{eff}$ =5E-19 cm$^2$/s

Table 2.4: Fluorescein simulated mass (mg) compared to average *in vitro* mass. Monolayer thickness of 5 µm, volume of 1.18E-03 mL. All mass multiplied by 1E-08.

| Time (hrs) | *In Vitro* (mg) | $D_{eff}$[a] (mg) | % error | $D_{eff}$[b] (mg) | % error |
|---|---|---|---|---|---|
| 6 | 26.5 | 2.43 | 90.85 | 12.1 | 54.24 |
| 9 | 26.7 | 3.64 | 86.35 | 18.2 | 31.74 |
| 18 | 29.1 | 7.28 | 75.01 | 36.4 | 24.96 |

[a] $D_{eff}$ =1E-18 cm$^2$/s
[b] $D_{eff}$ =5E-18 cm$^2$/s

NaFl, under an assumed 1 µm thickness, produced a decrease in percent error at the 6 and 9 hour time points for $D_{eff}$ from 5E-20 to 5E-19 cm$^2$/s and an increase in percent error at the 18 hour time point (Table 2.5). With a 5 µm monolayer thickness there is a decrease in all time points when the effective diffusion constant ($D_{eff}$) is increased from 5E-19 to 5E-18 cm$^2$/s (Table 2.6).

Table 2.5: NaFl simulated mass (mg) compared to average *in vitro* mass. Monolayer thickness of 1 µm, volume of 2.36E-04 mL. All mass multiplied by 1E-08.

| Time (hrs) | *In Vitro* (mg) | $D_{eff}$[a] (mg) | % error | $D_{eff}$[b] (mg) | % error |
|---|---|---|---|---|---|
| 6 | 6.29 | 0.607 | 90.35 | 6.07 | 3.54 |
| 9 | 6.44 | 0.91 | 85.86 | 9.10 | 41.39 |
| 18 | 6.51 | 1.82 | 72.04 | 18.2 | 179.59 |

[a] $D_{eff}$ =5E-20 $cm^2/s$
[b] $D_{eff}$ =5E-19 $cm^2/s$

Table 2.6: NaFl simulated mass (mg) compared to average *in vitro* mass. Monolayer thickness of 5 µm, volume of 1.18E-03 mL. All mass multiplied by 1E-08.

| Time (hrs) | *In Vitro* (mg) | $D_{eff}$[a] (mg) | % error | $D_{eff}$[b] (mg) | % error |
|---|---|---|---|---|---|
| 6 | 31.5 | 1.21 | 96.14 | 12.1 | 61.44 |
| 9 | 32.2 | 1.82 | 94.34 | 18.2 | 43.44 |
| 18 | 32.6 | 3.64 | 88.82 | 36.4 | 11.78 |

[a] $D_{eff}$ =5E-19 $cm^2/s$
[b] $D_{eff}$ =5E-18 $cm^2/s$

## 2.4 Discussion and Conclusion

For both fluorescein and NaFl tracers the *in vitro* data showed high fluorescence compared to FITC time points with few statistically significant increases in tracer uptake over the 24-hour period. Additionally, fluorescein and NaFl simulated diffusion models have trouble narrowing in on a suitable effective diffusion constant range due to very little change in the *in vitro* data. It is probable that the fluorescein and NaFl tracer mass could be better explained by a more appropriate mechanism other than the passive diffusion such as binding to the cell surface or embedding within the lipid bilayer. Only FITC showed an increase in *in vitro* tracer that could be closely recreated through computational simulation. For FITC, under a 1 µm thickness, effective diffusion constants between the range of 1.00E-20 and 5.00E-20 $cm^2/s$ can serve as a good approximation of *in vitro* data. At the 5 µm thickness, effective diffusion constants around 5.00E-19 $cm^2/s$ would serve as a good approximation for the *in vitro* data.

With minimal movement of FITC into the HBMEC monolayers, being shown above, an alternative computational approach would involve the use of the error function where the HBMEC monolayer could be modeled as a semi-infinite slab. The 1D partial differential equation (equation (2.6)) with the two boundary conditions (equations (2.7) and (2.8)) yield a diffusion equation (equation (2.9)) that can be used to describe the movement of FITC into the HBMEC monolayer as a function of space and time. Here, $c_0$ represents the surface concentration of tracer (0.1 mg/mL).

$$\frac{\partial c}{\partial t} = D_{eff}\frac{\partial^2 c}{\partial z^2} \tag{2.6}$$

$$c(0) = c_0,\ at\ surface\ (z = 0) \tag{2.7}$$

$$c(+\infty) = 0,\ at\ bottom \tag{2.8}$$

$$c(z,t) = c_0\,[1 - erf(\frac{z}{\sqrt{4tD_{eff}}})] \tag{2.9}$$

Fluorescent tracers have a multitude of uses in biomedical sciences to stain the exterior and interior of cells. This paper attempted to determine the potential magnitude of free diffusion of 3 tracers into HBMEC monolayers at different thicknesses of 1 and 5 µm. It was determined that although higher than FITC, both fluorescein alone and NaFl showed very little increase in tracer concentration from 3 hours to 24 hours while FITC continued to increase at statistically significant levels. Under the assumption of diffusion with no reaction and binding terms, fluorescein and NaFl effective diffusion constants were not able to be narrowed to produce simulated curves similar to the in vitro calibration data but a narrow range can be determined for FITC. This suggests that the retention of fluorescein and NaFl to the HBMEC monolayer may be better explained by another mechanism while FITC uptake make be reasonably approximated using a diffusion model. It is also important to note that *in vitro* results achieved are highly dependent on a multitude of experimental factors such as pH, temperature, cell type, and concentration levels.

## 2.5 Acknowledgements

We would like to thank the Virginia Tech Initiative for Maximizing Student Development (IMSD) program and the Virginia Tech Center for Autism Research (VTCAR) for partial support of this research project.

# Chapter 3

# Effect of Febuxostat on Oxidative Stress and Autistic Behaviors in BTBR Mice

**Jamelle M. Simmons, Wataru Ito, Alexei Morozov, Yong W. Lee**

**Submitted to Physiology and Behavior**

Autism spectrum disorder (ASD) is a lifelong neurodevelopmental disability that affects individuals in the areas of social interaction, verbal and non-verbal communication, and restrictive and repetitive behaviors. Xanthine oxidase (XO) is an enzyme involved in the conversion of hypoxanthine to xanthine with the resultant byproducts leading to elevated levels of reactive oxygen species (ROS) that can cause oxidative stress. With XO being found in multiple tissues, including the brain, we examined the use of febuxostat in the inhibition of XO in a BTBR mouse model and the potential benefits on oxidative stress and social behaviors. Juvenile C57BL/6J (C57) and BTBR T+ ltpr3tf/J (BTBR) male mice were treated with either a vehicle solution (5% dimethyl sulfoxide) or a vehicle solution + febuxostat at 10mg/kg for seven days. Changes in body and brain weight were recorded, general activity levels assessed, social interaction with demonstrator mice (129S1/SvlmJ) or novel objects (empty cup) quantified, and reactive oxygen species intensity measured by dihydroethidium

(DHE) staining. We found that the treatment of BTBR mice with febuxostat did not lead to statistically significant reductions in repetitive behaviors or improvements in social interaction. We also found that there were no significant differences between C57 control mice and BTBR vehicle or drug treated mice for levels of ROS. With febuxostat having a high binding affinity for plasma proteins, alternative delivery methods, such as the use of infusion pumps, may be needed to bypass the blood-brain barrier and expose brain tissue to high enough levels to allow for better evaluation of the potential of febuxostat for use in treating autism.

## 3.1 Introduction

Autism spectrum disorder (ASD) is a lifelong neurodevelopmental disability characterized by abnormalities in areas of (1) social interaction, (2) communication, and (3) restrictive and repetitive behaviors.[3,4] The exact cause of ASD is not known but research suggests that a multitude of factors may be at play such as (1) genetics,[16] (2) mitochondrial dysfunction,[18,119] (3) metabolic dysfunction,[20–22] (4) environmental,[23] and (5) oxidative stress.[24–26,120–123] Oxidative stress is defined as the imbalance between the pro-oxidative and antioxidant states where an imbalance in favor of a pro-oxidant state can lead to elevated levels of reactive oxygen species (ROS) that can lead to cellular damage.[124]

ROS molecules such as superoxide radicals, hydrogen peroxide, hydroxyl radical, peroxynitrite, and reactive carbonyls are generated from a number of sources; (1) NADPH oxidase, (2) nitric oxide synthase (NOS), (3) mitochondria, and (4) xanthine oxidase (XO).[124] Xanthine oxidoreductase (XOR) includes the forms xanthine dehydrogenase (XDH) and xanthine oxidase (XO) where the XO form leads to the generation of superoxide and hydrogen peroxide from the reduction of hypoxanthine and xanthine.[38,124–126] The enzyme XO is found in the plasma, brain, lungs, liver, small intestines, and kidneys of varying levels depending on the animal species[46–48] and has been implicated in brain tissue damage due to ischemia and reperfusion as well as many other tissues.[49,127]

Research by Zoroglu et al. found elevated levels of XO in blood samples of autistic adolescents in addition to elevated levels of thiobarbituric acid reactive substances (TBARS), and superoxide dismutase (SOD) compared to age matched controls.[39] This study demonstrates the presence of elevated levels of oxidative stress outside of brain tissue as well as elevated levels of XO. With the XO enzyme being found in tissues throughout the body, including the brain, there is the potential for it to play a role in the generation of ROS in brain tissue.

If XO is involved in significant levels of oxidative stress in brain tissues, there are XO-inhibitors currently on the market that can be used to reduce the activity of this enzyme. The XO-inhibitor allopurinol has been around for decades as the primary compound of choice in inhibiting XO in gout. Allopurinol is an analogue of hypoxanthine that when converted to oxypurinol is responsible for most of the inhibiting effect on XO. Both allopurinol and oxypurinol are purine inhibitors that can potentially interfere with purine metabolism of compounds other than hypoxanthine and xanthine. Uloric (febuxostat) is a newer compound that has higher potency than allopurinol and is a non-purine inhibitor with specificity for XO where it does not affect other purines.[50,51,128]

We hypothesize that elevated levels of XO result in an increase in oxidative stress which can lead to cellular damage in autistic brain tissue. Through use of febuxostat, XO levels would be inhibited which would lead to lower levels of cellular ROS generation and some recovery of typical behavior of autism. A mouse model of autism, BTBR T+ ltpr3tf/J (BTBR), was used in febuxostat treatments as it shows the most face validity to the diagnostic symptoms of autism: (1) reduced reciprocal social interactions, (2) low sociability, (3) increased repetitive self-grooming, (4) reduced social transmission of food preference, and (5) abnormal ultrasonic vocalizations.[129] Preliminary research from our lab has found elevated mRNA expression levels of XO in the brain tissue of 3 week old male BTBR mice (data not shown). The main goal of the present study is to determine if repeated dosing of febuxostat leads to reductions in XO-induced oxidative stress and improvements in behaviors of juvenile BTBR mice.

## 3.2 Materials and Methods

### 3.2.1 *Animals*

Three week old male C57BL/6J (C57) and BTBR T+ ltpr3tf/J (BTBR) mice and seven week old male 129S1/SvlmJ (129S1) mice were purchased from Jackson Laboratories (Bar Harbor, ME). Male juvenile mice were used for this study as prevalence rates in male children are higher than in female children.[1] C57 and BTBR mice were housed individually while 129S1 mice were housed in groups. All cages were supplemented with water gels and enrichment toys in addition to access to food and water ad libitum. Mice were placed on a 12 hour light/dark cycle for the entire study. This study was carried out in accordance with the Guide for the Care and Use of Laboratory Animals and the approved Virginia Tech Institutional Animal Care and Use Committee (IACUC) protocol (number 16-003). All surgical procedures were performed under anesthesia, 2.5% Avertin solution at 0.17mL/10gram body weight through intraperitoneal (I.P.) injection, and all efforts were made to minimize distress and suffering.

### 3.2.2 *Treatment by Intraperitoneal Injection*

Mice were split into three groups, (1) C57 + Vehicle, (2) BTBR + Vehicle, and (3) BTBR + Febuxostat (drug) with a sample size of 5 mice per group. The vehicle solution was composed of dimethyl sulfoxide (DMSO) diluted to a final concentration of 5% (v/v) in sterile phosphate buffered saline (PBS 1x) before I.P. injection. Febuxostat was diluted in the vehicle solution and injected at a concentration of 10mg/kg per mouse in the volume of 0.1 to 0.21 ml. All groups were dosed once a day for 7 days.

### 3.2.3 *Behavioral Testing*

#### *Room Preparation*

All mice were transported to the testing room and given 1 hour to acclimate to the environment. C57 and BTBR groups were housed on racks outside of the testing environment while the 129S1 mice were held in the testing room to avoid contact with other mice. The testing room was set up with a three-chamber sociability apparatus made of Plexiglas with cameras placed in front, behind, and above the apparatus. Removable dividers were placed to separate all three chambers and wire cups were placed in the left and right chambers while the middle chamber remained empty. The lights were dimmed to 90 Flux and a curtain was used to hide the experimenter from the animals.

#### *Three-Chamber Testing*

Testing occurred in two phases with 10 minute durations using an adapted protocol.[130–132] During phase 1 an experimental mouse (C57 or BTBR) was placed in the middle chamber with the removable dividers in place to restrict movement for 10 minutes. During phase 2, a 129S1 demonstrator (novel) mouse was placed under an inverted wire cup in either the left or right chambers. For each new experimental mouse the location of the demonstrator mouse was switched between the left and right chambers. In the remaining chamber an empty inverted wire cup served as a novel object. Both wire cups had another object (cup filled with water) placed on top to keep the experimental mice from climbing on top of the cups during phase 2 testing. With the cups in position, the dividers separating the chambers were removed and the experimental mouse was given access to all three chambers for 10 minutes. During both testing phases cameras were used to record movement and behaviors that were later analyzed off line. At the end of phase 2 the experimental and novel mice

were returned to their cages. The interior of the apparatus was cleaned with 70% ethanol followed by water and towel dried after each experimental mouse was used. The wire cups were cleaned with water and towel dried for the next experimental run.

### 3.2.4 *Quantification of Behaviors*

Repetitive grooming was quantified during phase 1 of testing. Only grooming bouts occurring for 1 second or longer were counted towards the cumulative scoring. During phase 2 of testing, the following parameters were quantified: (1) total number of crossings between chambers, (2) total time spent in each chamber, (3) total time spent around the cup with the demonstrator mouse vs. the novel object, (4) total social approach time where the experimental and demonstrator mouse were face-to-face, and (5) total time spent grooming when given access to all chambers.

### 3.2.5 *Reactive Oxygen Species (ROS) Measurement*

The day following behavioral testing, mice brains were perfused with ice-cold PBS 1x with 6 units of heparin per ml of PBS solution. Brains were cut into right and left hemispheres down the midline (anterior to posterior) through the corpus callosum. Hemispheres were frozen on dry ice and stored at -80°C until analysis. Next, frozen brain sections were placed in 20% sucrose solution in PBS 1x overnight until hemispheres sunk. Next brain hemispheres were botted and embedded in optimum cutting temperature (OCT) compound and frozen. Brain hemispheres were cut into 20 micron (µm) sections starting at the midline where the hemisphere was initially cut moving laterally into the parietal-temporal lobes. Sections were mounted on glass slides and stored at -20°C until use.

For dihydroethidium (DHE) staining slides were thawed to room temperature and washed in

PBS 1x to remove OCT. Next, slides were dried and sections were outlined with a liquid pap pen. DHE solution was added to brain sections and incubated in the dark for 30 minutes at 37°C. The solution was then removed and sections were imaged at 20x within 1 hour of incubation with 4 images taken per section for fluorescence intensity quantification with Image J. Two sections were used from samples near the midline and two sections were used further into the parietal-temporal lobes 360 microns away from the midline sections. The DHE stain is reactive with ROS, the imbalance of the pro-oxidant and antioxidant states can lead to oxidative stress if there are more pro-oxidant species than the cell can handle.

### 3.2.6 *Statistical Testing*

For behavioral testing each group contained 5 animals. Tests for equal variance and normality were run to determine if a parametric ANOVA could be used to compare more than two groups. Post-hoc Tukey multiple comparisons were run when the ANOVA reported p-values less than 0.05. Numerical values reported were mean ± standard error for each tests. In figures statistical differences less than 0.05 were denoted with a single asterisk (*) while p-values less than 0.01 were denoted with two asterisk (**) and p-values less than 0.001 were denoted with three asterisks (***). All statistics were generated using Minitab 18.

## 3.3 Results

### 3.3.1 *Effects of Febuxostat on Body and Brain Weight*

All mice were initially weighed before the IP injection schedule began as well as the end of the study under anesthesia before tissue collection took place. C57 mice saw an increase in average weight from 9.8 ± 0.2 to 18.2 ± 0.374 grams over 7 days while the BTBR vehicle

group saw increases from 15 ± 0.447 to 25.4 ± 0.678 grams and the BTBR drug group saw increases from 15.6 ± 0.4 to 25.2 ± 0.58 grams. Very little variation in whole brain weight was found between all groups. C57 mice, on average, had a brain weight of 0.44 ± 0.009 while the BTBR vehicle and drug groups had average brain weights of 0.41 ± 0.025 and 0.41 ± 0.012 grams. Under vehicle and drug treatments all groups saw a significant increase in weight gain over 7 days with p-values of <0.0001 (Figure 3.1A) and no statistically significant differences in brain weight were noted between groups using an ANOVA (F-stat = 0.98, p-value = 0.402) comparing the means of each group (Figure 3.1B).

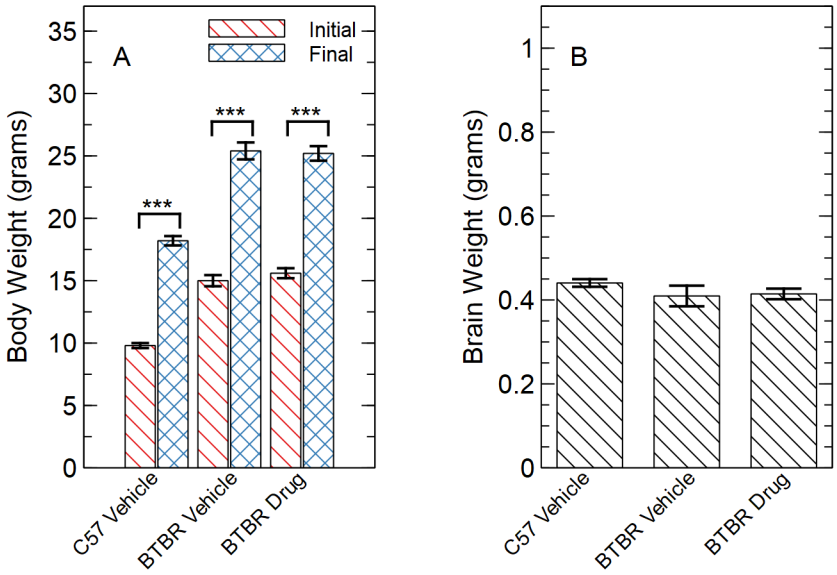


Figure 3.1: Body weight and brain weight of juvenile mice. (A) Body weight average of C57 and BTBR groups at 3 and 4 weeks of age (n=5 per group). Significant increases in weight gain were observed between weeks 3 and 4 for each group with a p-value <0.0001. (B) Whole brain weight average of C57 and BTBR groups at 4 weeks (n=5 per group). No significant differences in average brain weight were found between the groups using an ANOVA (F-stat = 0.98, p-value = 0.402).

### 3.3.2 *Effects of Febuxostat on General Activity Levels*

General activity levels of mice were assessed by counting the number of chamber crossings over a 10 minute period to determine if febuxostat had any sedative effects beyond the effects of DMSO. Significant differences in activity levels were found between the groups (ANOVA F-stat = 9.89, p-value = 0.003) with Tukey post-hoc comparisons showing p-values of 0.005 and 0.007 when comparing C57 activity levels to the BTBR vehicle and febuxostat groups respectively (Figure 3.2). No significant differences were noted between the vehicle and febuxostat groups for BTBR mice.

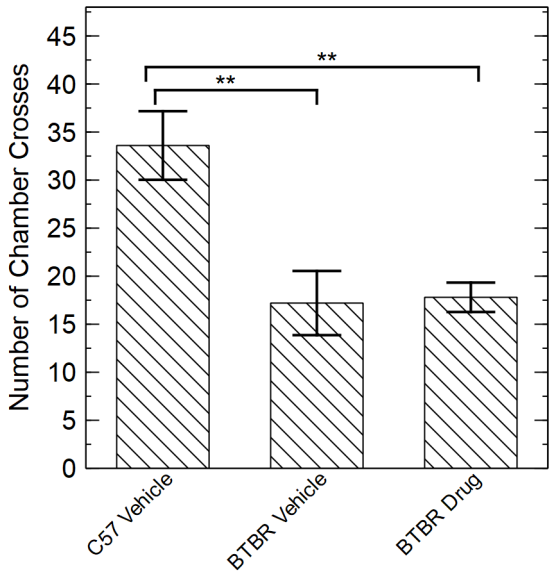


Figure 3.2: Chamber crossings general activity levels. Significant reductions in activity levels were detected between the C57 vehicle group and both the BTBR vehicle and drug groups with p-values of 0.005 and 0.007 respectively.

### 3.3.3 *Effects of Febuxostat on Grooming Behaviors*

Each group of experimental mice were assessed for grooming activity when isolated to the center chamber (restricted) for 10 minutes and when given free access to all chambers (un-

restricted) for 10 minutes (Figure 3.3). In the unrestricted setting grooming was counted if it occurred in any of the three chambers. Within all groups there were no statistically significant differences noted between the restricted and unrestricted settings. Between groups no statistically significant differences were found in the restricted setting using an ANOVA (F-stat = 0.02, p-value = 0.985). A significant increase in grooming was found between groups in the unrestricted setting with an ANOVA (F-stat = 4.03, p-value = 0.046) showing a higher tendency for grooming in the BTBR group receiving the drug treatment compared to the C57 vehicle group using Tukey post-hoc comparisons (T-value = 2.83, p-value = 0.037).

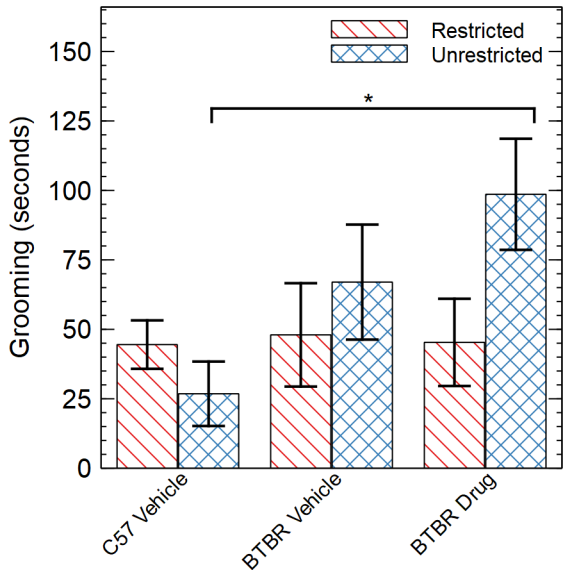


Figure 3.3: Phase 1 (restricted) and phase 2 (unrestricted) grooming activity. A higher tendency of grooming was noted in the BTBR group receiving the drug treatment, in the unrestricted setting, compared to the C57 vehicle group (p-value = 0.037).

### 3.3.4 *Effects of Febuxostat on Time Spent in Chambers*

For the C57 group significant differences were noted between time spent in each chamber (ANOVA F-stat = 19.78, p-value = 0.00016) (Figure 3.4). Using a Tukey post-hoc compari-

son a significantly higher portion of time was spent in the demonstrator chamber compared to the empty chamber (p-value = 0.01) and the middle chamber (p-value = 0001). For the C57 group significantly more time was spent in the middle chamber compared to the empty chamber with a p-value of 0.047. For the BTBR vehicle group significant differences in time spent in each chamber were detected (ANOVA F-stat = 4.26, p-value = 0.04). Using a post-hoc Tukey comparison significantly more time was spent in the demonstrator chamber than the middle chamber (p-value = 0.033). In the BTBR febuxostat group significant differences were detected between chamber times (ANOVA F-stat = 17.98, p-value = 2.3E-06). Using a post-hoc Tukey comparison significantly more time was spent in the demonstrator than the middle chamber (p-value = 1.2E-05) and significantly more time was spent in the empty chamber than the middle chamber (p-value = 4.5E-04).

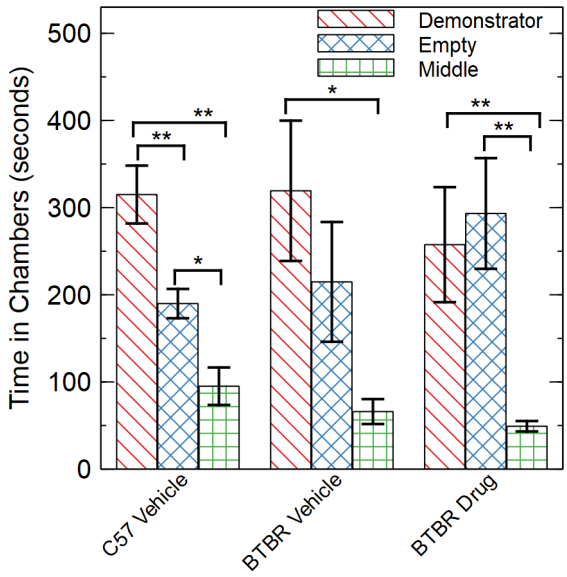


Figure 3.4: Time spent in each chamber. The C57 group spent significantly more time in the demonstrator chamber than both the middle and empty chambers. The BTBR vehicle group spent significantly more time in the demonstrator chamber than the middle chamber. The BTBR febuxostat group spent significantly more time in the demonstrator and empty chambers than the middle chamber.

### 3.3.5 *Effects of Febuxostat on Time Spent with Demonstrator and Empty Cups*

All groups were assessed for time spent around the empty cup versus time spent around the cup with the demonstrator mouse while given unrestricted access to all chambers for 10 minutes (Figure 3.5). Times were counted if the mice were close to the wire cups. The C57 group spent significantly more time around the cup with the demonstrator mouse than the empty cup (p-value = 0.024). No significant differences were noted within the BTBR vehicle and febuxostat groups with p-values of 0.3 and 0.584 respectively.

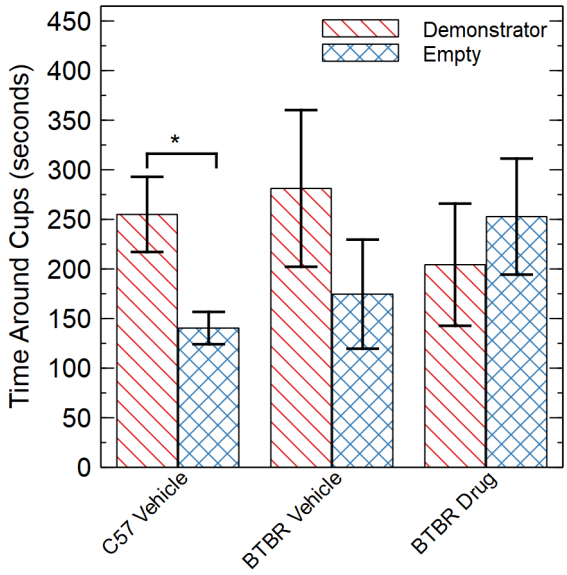


Figure 3.5: Time spent around empty and demonstrator cups. The C57 group spent significantly more time around the demonstrator cup than the empty cup. BTBR groups showed no significant differences in time spent in around empty and demonstrator cups.

### 3.3.6 *Effects of Febuxostat on Social Interaction*

During phase 2 when experimental mice were given free access to all chambers, the amount of time spent face to face with the demonstrator mouse was quantified (Figure 3.6). C57

mice, on average, spent 24.17 ± 6.15 seconds interacting with the demonstrator mouse. The BTBR vehicle group and BTBR drug groups spent 3.42 ± 1.65 and 3.92 ± 2.11 seconds on average interacting with the demonstrator mice. When comparisons were made between groups for time spent interacting with demonstrator mice differences were found between all three groups (ANOVA F-stat = 9.35, p-value = 0.004). A post hoc Tukey comparison shows the C57 group having spent significantly more time with the demonstrator mice that the BTBR vehicle group (p-value = 0.007) and the BTBR drug group (p-value = 0.008).

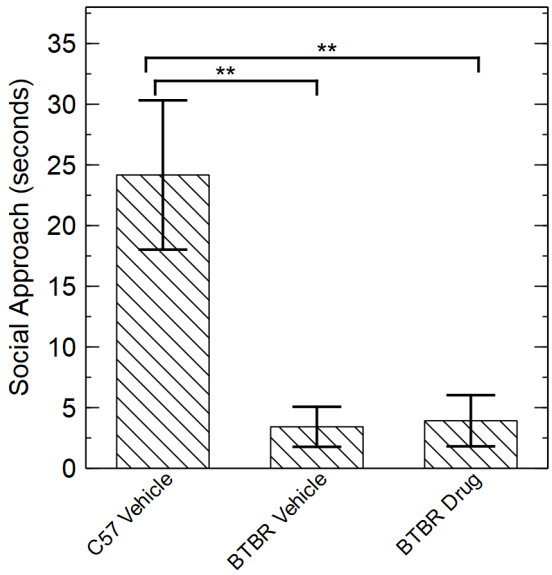


Figure 3.6: Face-to-face interaction with demonstrator mice. The C57 mice spent significantly more time face to face with demonstrator mice than both BTBR groups.

### 3.3.7 *Effects of Febuxostat on Reactive Oxygen Species (ROS)*

Fluorescence intensities were quantified in all groups for samples taken near the brain midline (medial) and laterally from the midline into the parietal-temporal lobes (at 360µm from the midline sections) using a DHE staining (Figure 3.7). All intensities were averaged from each group for a total of 4 sections quantified per animal in quadruplicate with 5 animals per

experimental group. The C57 group had an average fluorescent intensity of 978.9 ± 29.3 and the BTBR vehicle and drug groups had average intensities of 1027.3 ± 24.8 and 989.5 ± 28.5 respectively. An ANOVA between the three groups showed no significant differences in fluorescent intensities (F-stat = 0.85, p-value = 0.428).

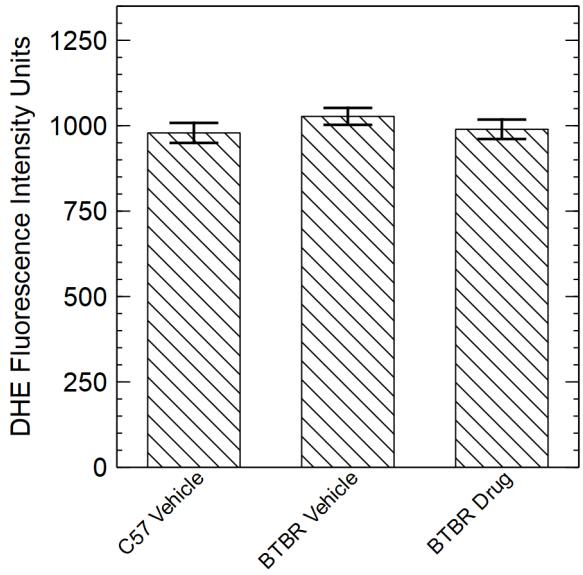


Figure 3.7: DHE fluorescent intensity of brain tissue. No significant differences were noted between groups.

## 3.4 Discussion

The aim of the study presented was to determine if the use of XO inhibitors could improve behavioral deficits in a BTBR mouse model by reducing oxidative stress. Juvenile male BTBR mice, 3-4 weeks in age, were treated with febuxostat for 7 days followed by behavioral assessment and quantification of ROS levels in brain tissue. Overall, we found no statistically significant improvements in behaviors with drug administration compared to BTBR vehicle and C57 vehicle controls.

With repeated administration of vehicle solutions (DMSO and PBS) and vehicle + febuxostat (10mg/kg) solutions we tracked the body weight and brain weight of the C57 and BTBR controls (vehicle solution) and the BTBR experimental group (vehicle + febuxostat). In all groups there were significant increases in body weight from the start of I.P. injections (initial) and the end of I.P. injections (final) which shows that the administration of the vehicle and febuxostat did not have a negative impact on the growth of the juvenile mice. The difference in body weight between the C57 and BTBR mice could be explained by the rapid growth weight seen in BTBR mice post-natal days 2 to 12.[133] Brain weights were measured, at 4-5 weeks of age, to determine if there was any loss in brain mass between the groups and no differences were found. Both measures were used to determine overall animal health for behavioral testing.

During phase 2 of testing in the three-chamber apparatus, the general activity levels of mice were quantified by the number of crosses between chambers made in a 10 minute period. This measure was used to determine if febuxostat has any stimulant or sedative effects on the BTBR mice. There were no significant differences found between the BTBR mice activity levels from the vehicle and vehicle + febuxostat groups. There was a significantly higher level of cage crossings seen when comparing the C57 group to the BTBR groups, but this can be attributed to strain differences.

Repetitive grooming in BTBR and C57 groups were assessed in the three-chamber apparatus in two phases where in phase 1, the mice were restricted to the center chamber, and in phase 2, the mice were given free access to all portions of the chamber that included a novel mouse under a wire cup or an empty wire cup. Pearson et al.[134] found higher levels of repetitive grooming in adult BTBR mice compared with adult C57 mice when restricted to a clear Plexiglas chamber for 30 minutes. Our study found no significant differences between groups when restricted to the center chamber of the Plexiglas three-chamber apparatus for

10 minutes. Repetitive grooming was also monitored during phase 2 of testing to determine if exposure to new environmental stimuli (empty cup and demonstrator mouse) would influence levels of grooming. The C57 group showed a decrease in repetitive grooming and the BTBR groups showed increases in grooming with a significantly higher amount of grooming found in the BTBR (febuxostat) group compared to the C57 (vehicle) group but no significant differences detected between the BTBR groups.

Time spent in each of the three chambers was measured for all groups to determine if there was a preference for being in an empty chamber, chamber with an empty cup (novel object), or chamber with the demonstrator mouse. Result of our study, within groups, show that C57 mice have a preference for spending time in the chamber with the demonstrator mouse compared to the chamber with the empty cup (novel object) while the BTBR (vehicle) mice showed no preference between the two chamber which is consistent with previous research in adult and juvenile C57 and BTBR mice.[135,136] The addition of febuxostat did not improve chamber preference of BTBR mice to favor the chamber with the demonstrator mouse over the empty cup (novel object).

Time spent around the demonstrator and empty cups were also measured as a more sensitive measure compared to time spent in each chamber. Mice are able to be in close proximity to the cups without directly engaging in social interaction with demonstrator mice. The C57 mice showed a significant preference for spending time around the demonstrator cup while the BTBR groups showed no statistically significant preference for either cup.

The final test for sociability (social approach) was used as the most sensitive measure of social interaction where experimental mice were engaged in face-to-face sniffing with the demonstrator mice. Our results showed that the C57 mice spent significantly more time engaged in face-to-face sniffing of the demonstrator mice than the BTBR (vehicle) mice which is consistent with previous juvenile mice research by Babineau et al.[135] The addition of

febuxostat treatment in BTBR mice did not improve social interaction of BTBR (febuxostat) mice compared to BTBR (vehicle) mice. C57 mice had a significantly higher amount of time engaged in sniffing compared to the BTBR (febuxostat) mice as well.

Currently there no supportive data to determine if BTBR mice were systemically exposed to febuxostat leaving us unable to determine if the drug had any behavioral effects over the 1 week treatment period. Additionally, the study design had a low sample size per group resulting in low overall power. Using a two-sample power analysis between BTBR (febuxostat) and BTBR (vehicle) for grooming (restricted), grooming (unrestricted), and social interaction (face-to-face), estimated samples sizes required to detect differences can be calculated. Here we can assume equal sample sizes per group, a power of 0.80, and an alpha of 0.05 to get an idea of the number of animals needed. For grooming (restricted) assuming a mean difference of 10 seconds between the BTBR groups and a standard deviation (SD) of 35 seconds yields an effect size of 0.29 which results in a sample size of 188 mice per group to achieve an overall power of 80%. In the grooming (unrestricted) setting we can assume a mean difference of 20 seconds between the BTBR groups and a standard deviation (SD) of 45 seconds yields an effect size of 0.44 which results in a sample size of 83 mice per group to achieve an overall power of 80%. For social interaction (face-to-face) assuming a mean difference of 5 seconds between the BTBR groups and a standard deviation (SD) of 4 seconds yields an effect size of 1.25 which results in a sample size of 12 mice per group to achieve an overall power of 80%. Overall, we would need more mice to detect differences in repetitive grooming behaviors than for social interaction.

DHE staining of mouse brain tissue was carried out for all three groups to determine if ROS levels would be lowered with febuxostat treatment. Overall, the levels of ROS in all three groups were not significantly different from each other; this result requires further investigation. If febuxostat managed to cross the blood brain barrier (BBB) into the brain

tissue to inhibit XO it would be expected that lower levels of ROS would be present when comparing the BTBR (febuxostat) to the BTBR (vehicle) groups but that was not seen. Questions remain on (1) whether febuxostat made it to the blood stream after I.P injection and (2) if febuxostat was absorbed into the blood stream was it able to reach the brain tissue? Assuming that febuxostat could make it into the blood stream it is possible that it would not be able to cross the BBB after 7 days of administration due to the properties of the drug and properties of the BBB. Factors important in determining if a compound will cross the BBB are its size, charge, lipophilicity, tertiary structure, and its amount of protein binding.[88,137] In humans, febuxostat has a rapid absorption after oral administration where it reaches peak concentrations in the plasma within 1 hour and has high binding to albumin in the blood of approximately 99%.[75,80] With plasma proteins such as albumin not being able to cross the BBB[138] it is expected that compounds bound to these proteins would also not be able to cross the BBB which may help explain why differences were not found between BTBR groups.

## 3.5 Conclusions

With febuxostat being highly bound to plasma proteins, specifically albumin, a direct delivery route into brain tissue may be needed to study the potential effects of febuxostat on ROS levels. Micro-infusion systems can be implanted into mice that allow for direct access to the brain where compounds can be delivered continuously for extended periods of time.[139,140] This approach would be favorable as it would remove the need for daily administration through I.P. injections and longer studies can be run where delivery of febuxostat into brain tissue is ensured.

## 3.6 Acknowledgements

We would like to thank Molly Accord and Richard Yea for their help with tissue collection, tissue processing, and data entry.

# Chapter 4

# Pharmacokinetic Modeling of Absorption, Distribution, Metabolism, and Excretion of Febuxostat

**Jamelle M. Simmons, Luke Achenie, Yong W. Lee**

**In preparation for submission**

Febuxostat is a non-purine selective inhibitor for xanthine oxidase management in gout patients with rapid absorption and low to medium volume of distribution. It is metabolized by both the cytochrome P450 and uridine diphosphate (UDP) glucuronosyltransferases (UGT) families in the liver, specifically UGT1A1, 1A3, 1A7, 1A8, 1A9, 1A10, and CYP1A1, 1A2, 2C8, and 2C9. While febuxostat is targeted for gout management, alterations in blood-brain barrier (BBB) integrity, found in some neurological diseases, can see increased permeability into the central nervous system (CNS). Brain tissue also contain cytochrome P450 enzymes and the ability to metabolize drugs. This study models pharmacokinetic (PK) absorption, distribution, metabolism, and excretion beyond the central plasma compartment under multiple hypotheses to explain drug movement into other compartments.

Human plasma data at 40mg and 80mg febuxostat dosages from Luo et al.[76] were digitized and a multi-compartment model constructed under four cases where peripheral compartments (liver, CNS, kidney, and other tissues) were optimized to produce a simulated plasma compartment that closely matched human plasma data. A total of four hypothesis-driven cases are proposed (1) drug movement into all compartments, (2) no drug passage into the CNS, (3) metabolism and excretion only occur in the liver and kidney compartments, and (4) a diseased state in the CNS with increased permeability.

Cases 1 and 2 produced PK models that resulted in a simulated central plasma compartment that had low percent error for area under the curve (AUC) where rates of entry into compartments were either equal to or higher than exit rates back to the central plasma compartment. Cases 3 and 4 were only able to produce simulated central plasma data similar to human data by creating exiting rates at significantly higher levels than entry rates for the CNS and tissue compartments. Case 1 emerged for further investigation to continue to narrow PK parameters of peripheral compartments when permeability and metabolism in the CNS are considered.

## 4.1 Introduction

Febuxostat (MW = 316.374), 2-[3-cyano-4-(2-methylpropoxy)phenyl]-4-methylthiazole-5-carboxylic acid, is a non-purine selective inhibitor of xanthine oxidase for the management of hyperuricemia in patients with gout[75,77,83]. In healthy human subjects, febuxostat is rapidly absorbed after oral administration with peak concentrations reached after 0.5 – 1.5 hours under fasting conditions. Additionally, febuxostat is a weak acid with a dissociation constant (pKa) of 3.3, is highly bound to albumin in blood (approximately 98-99%) and carries a low to medium volume of distribution[75,77]. Pharmacokinetic (PK) parameters calculated from human data are highly variable in literature even among studies drawing from the same population (Table 4.1).

Table 4.1: Pharmacokinetic data of febuxostat plasma levels in healthy volunteers.

| Parameters | Dose | Zhou et al.[a] ([84]) Mean±SD | Zhang et al.[a] ([79]) Mean±SD | Wu et al.[b] ([85]) Mean±SD |
|---|---|---|---|---|
| $C_{max}$ (ng/ml) | 40mg | 2835±1136.41 | 1911.95±678.40 | 3318±1446 |
| | 80mg | 5356.75±1711.33 | 2966.70±1176.13 | 4519±1968 |
| $t_{max}$ (hr) | 40mg | 1.71±0.75 | 1.02±0.72 | 1.5±0.8 |
| | 80mg | 1.46±0.62 | 0.96±0.35 | 2.9±1.9 |
| $t_{1/2}$ (hr) | 40mg | 5.95±2.71 | 3.81±1.77 | 4.7±1.8 |
| | 80mg | 9.41±7.47 | 5.02±1.23 | 6.5±2.3 |
| CL/F (L/hr) | 40mg | 4.81±1.18 | 9.41±2.87 | not specified |
| | 80mg | 4.70±1.21 | 10.92±4.66 | not specified |
| Vd/F (L) | 40mg | 39.66±16.69 | 48.80±19.49 | not specified |
| | 80mg | 62.72±51.41 | 77.90±32.35 | not specified |

[a] healthy male and female Chinese volunteers under fasting conditions
[b] no gender or fasting specifications of healthy Chinese volunteers

Metabolism of drugs occurs by phase I and phase II elimination where phase I generally leads to oxidation, reduction, or hydrolysis of drugs while phase II leads to conjugation reactions which helps with excretion of metabolites in the urine[69].Cytochrome P450s (CYP450s) enzymes are responsible for most of the phase I drug metabolism and are mainly present on

smooth endoplasmic reticulum (ER) and mitochondria of liver hepatocytes and small intestine of epithelial cells. Based on the protein content, CYP3A4 is the most abundant in the human liver at 22.1%, followed by CYP2E1 at 15.3%, and CYP2C9 at 14.6%, with CYP2C8, CYP1A2, and other CYP450s accounting for smaller percentages[70]. The uridine diphosphate (UDP) glucuronosyltransferase (UGT) family is responsible for phase II conjugation where compounds are glucuronidated. The liver is the main site of glucuronidation although other tissues such as the kidney, lung, gastrointestinal tract, prostate, spleen, skin, and brain also express UGT[73].

Febuxostat is extensively metabolized by both the UGT and CYP450 enzymes, specifically UGT1A1, 1A3, 1A7, 1A8, 1A9, 1A10, and 2B7 by conjugation and CYP1A1, 1A2, 2C8, and 2C9 by oxidation[75,141,142]. Phase I metabolism results in up to 40% metabolism by glucuronidation and up to 35% metabolism by oxidation[77,80,83]. While the focus of metabolism of febuxostat has mainly centered on the gastrointestinal system, oxidation of drug compounds can also occur in other tissues such as the brain. Although the brain CYP levels have been estimated to range from 0.5-2%[71] up to approximately 10%[72] of those found in the liver they can still contribute to metabolism of drugs that can reach brain tissue. Of the CYPs found to metabolize febuxostat in the liver, CYP1A1, 1A2, and 2C8 have been shown to be expressed in the brain in various regions such as the cortex, cerebellum, basal ganglia, hippocampus, substantia nigra, medulla oblongata, and other tissues[143,144].

Normally, the blood-brain barrier (BBB) of the central nervous system (CNS) is extremely selective in the types of compounds that cross it and the mechanism of transport. During a diseased state the BBB can have increased permeability which would allow compounds that previously would not be able to cross the BBB. BBB disruption and altered function have been documented in autism spectrum disorder (ASD)[68], multiple sclerosis (MS)[64,65], and Alzheimer's disease (AD)[64,67]. As these disorders remain with patients from their early

onset it is important to also investigate drug transport into the CNS space when the BBB function is altered.

With the potential of the brain to metabolize febuxostat PK models can be developed that include the CNS as another site where drugs can be distributed if they reach the central plasma compartment. With pharmacological data on human organ systems being sparse outside of drug concentrations in blood (specifically plasma), computational approaches can be used to simulate and evaluate hypotheses about how various systems interact when drug flows throughout the body. We attempt to determine pharmacologic parameters outside of the blood plasma through the use of PK models represented through linear differential equations where we link the plasma compartment to the liver, kidneys, CNS, and remaining tissues. The goal of the study is to estimate PK parameters for peripheral compartments that yield a simulated plasma compartment similar to human published data.

We investigated 4 hypothesis-based cases as follows: (1) drug flow to the plasma compartment and all other compartments, (2) drug flow to the plasma compartment assuming no metabolism in the CNS, (3) drug flow to the plasma compartment assuming no metabolism in both the CNS and other tissues, and (4) drug flow to the plasma compartment assuming increased drug flow into the CNS but no metabolism in the CNS. All cases were simulated for both 40 and 80mg febuxostat doses which are approved for use in humans. For this study no distinction was made between unchanged febuxostat or its active oxidized metabolites 67M-1, 67M-2, or 67M-4 in the compartments.

## 4.2 Materials and Methods

### 4.2.1 *Plasma Pharmacokinetic Parameters*

Luo et al.[76] conducted a 4-way, randomized, open-label cross-over clinical study in 24 healthy male volunteers (age 18 to 40 years) with a body mass index between 19-24 kg/m$^2$. Blood samples were collected at 0, 0.25, 0.5, 0.75, 1.0, 1.5, 2, 3, 4, 6, 8, 10, 12, 16, 24, 36, and 48 hours (hr). For the 40mg and 80mg reference formulations the time to reach maximum serum concentrations ($t_{max}$) was 1.85±1.03 (mean ± SD) hours and 2.23±1.55 hours for the 40 and 80mg doses respectively. The apparent volume of distribution (V/F) was 53.61±22.33 liters (L) and 63.77±23.74 L for the 40 and 80mg doses. The clearance (CL/F) was 8.01±2.91 liters per hour (L/hr) and 8.32±2.69 L/hr for the 40 and 80mg doses respectively[76].

For our purposes the PK mean clearance values from Luo et al.[76] were rounded to 8 L/hr for both 40 and 80mg doses. Volume of distribution was rounded to 54 L for the 40mg dose and 64 L for the 80mg dose. The elimination rate from the plasma compartment, $k_{el}$(hr$^{-1}$), was calculated by dividing Cl/F by V/F for both the 40mg and 80mg doses to yield elimination rates of 0.148 and 0.125 (hr$^{-1}$) for the 40 and 80mg doses respectively. The absorption rate ($k_a$, hr$^{-1}$) from the gastrointestinal tract into the plasma compartment for the 40 and 80mg doses was determined using the $t_{max}$ equation (equation(4.1)) where $t_{max}$ was set to 1.85 and 2.23 hr for the 40 and 80mg doses and $k_a$ was solved for. Absorption rates ($k_a$) were calculated as 1.34 and 1.1 (hr$^{-1}$) for the 40 and 80mg doses.

In a separate study Hira et al.[145] generated a population PK model for patients with severe renal impairment where a final model estimate for $k_a$ of 2.52 (hr$^{-1}$) was determined. Hirai et al.[146] assumed a value of 2.18 (hr$^{-1}$) for gastrointestinal absorption ($k_a$) as they were unable

to determine an absorption value. Both studies used absorption values higher than those determined from using the Luo et al.[76] data. The central plasma compartment terminal elimination rates ($k_{el}$), based on the Luo et al.[76] data, were calculated as 0.148 ($hr^{-1}$) for the 40mg single dose and 0.125 ($hr^{-1}$) for the 80mg single dose of febuxostat. PK studies, where $k_{el}$ values were published for a 80mg single dose, showed $k_{el}$ values of 0.086±0.030 ($hr^{-1}$) from Kim et al.[86] and 0.10996 ($hr^{-1}$) from Chandu et al.[147], which are both lower than the $k_{el}$ value for the 80mg single dose of febuxostat in this current study.

$$t_{max} = \frac{\ln\left(\frac{k_a}{k_{el}}\right)}{k_a - k_{el}} \tag{4.1}$$

WebPlotDigitizer version 4.1 https://automeris.io/WebPlotDigitizer was used to extract concentrations at each time point from the 40 and 80mg reference formulation plots from Luo et al. and the area under the curve (AUC) for both formulation was calculated using the trapezoidal method. Peak concentrations (ng/mL) from the digitized plots of the 40mg and 80mg doses were 1123 and 1796 respectively with AUCs of 5446.40 and 11026.95 (ng*hr/mL) respectively for the 40mg and 80mg doses.

### 4.2.2 *Development of a Multi-Compartment Pharmacokinetic Model*

A five compartment model (Figure 4.1) is developed with absorption of febuxostat into the central plasma compartment and bi-directional flow into the liver, kidneys, CNS, and all other tissues (fat, muscle, *etc.*). The PK parameter rates entering the CNS from the central compartment, returning to the central compartment, and metabolism in the CNS compartment are $k_{c1}$, $k_{c2}$, and $k_{cex}$ respectively (units, $hr^{-1}$). The parameters rates entering the liver from the central compartment, returning to the central compartment, and metabolism

in the liver compartment can be represented as $k_{l1}$, $k_{l2}$, and $k_{lex}$ respectively (units, $hr^{-1}$). The kidneys can be represented with parameter rates entering the compartment from the central compartment ($k_{k1}$), returning to the central compartment ($k_{k2}$), and being excreted from the body as $k_{kex}$ respectively (units, $hr^{-1}$). Parameter rates entering all other tissues from the plasma compartment, returning to the plasma compartment from the tissues, and retention in the tissues can be represented by $k_{t1}$, $k_{t2}$, and $k_{tex}$ respectively (units, $hr^{-1}$).

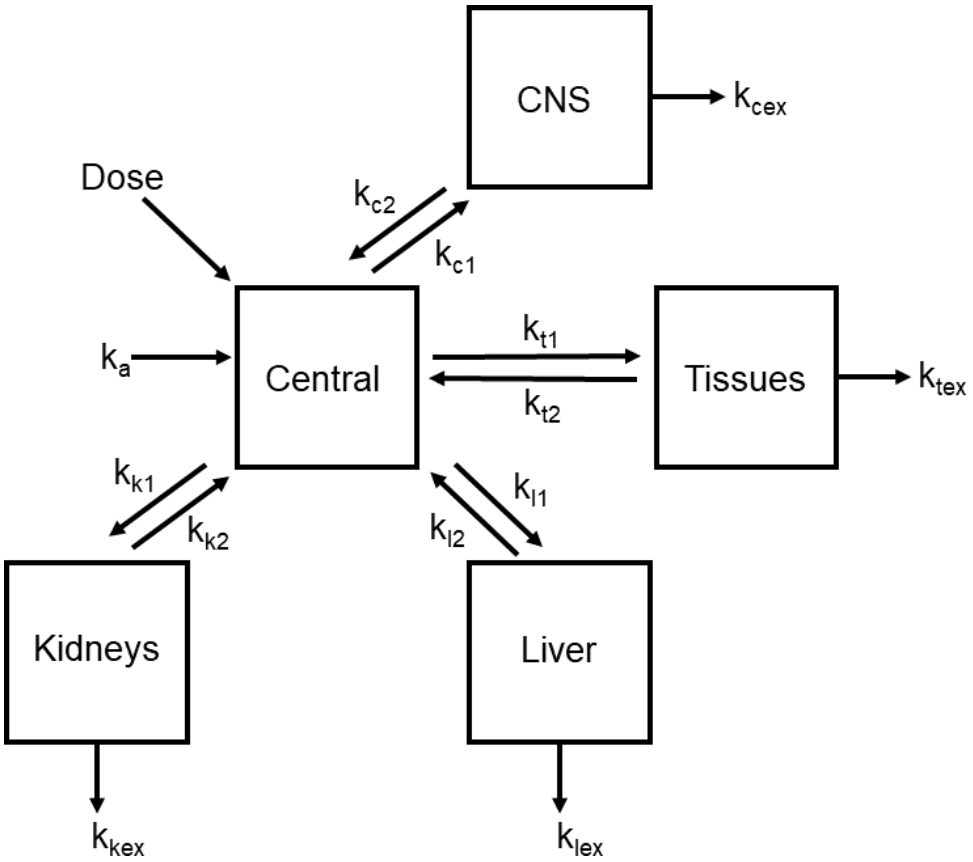


Figure 4.1: Pharmacokinetic model of febuxostat distribution in vivo for 40mg and 80mg cases. Bioavailability of 80% is assumed for both 40mg and 80mg cases.

The oral bioavailability of febuxostat is not known as there is no intravenous formulation to compare to the oral formulation but bioavailabilities have been assumed within the range of 65%[146] to 85%[77]. For modeling purposes we assumed an oral bioavailability of 80% for both the 40 and 80mg doses meaning that 80% of the dose made it to the central compartment

while the remaining 20% was removed from the body as waste.

The plasma compartment was exposed to the available dose of febuxostat continuously for times less than tmax for both 40 and 80mg doses (equation(4.2)). PK equations were generated for the CNS (equation(4.3)), tissues (equation(4.4)), liver (equation(4.5)), kidneys (equation(4.6)), and the central plasma (equation(4.7)) compartments. It is assumed that drug concentrations within each compartment are homogeneous at each time point.

$$R(t) = Dose \times Bioavailability,\ for\ t < t_{max} \tag{4.2}$$

$$\frac{d[CNS]}{dt} = k_{c1} \times Central - CNS[k_{c2} + k_{cex}] \tag{4.3}$$

$$\frac{d[Tissue]}{dt} = k_{t1} \times Central - Tissue[k_{t2} + k_{tex}] \tag{4.4}$$

$$\frac{d[Liver]}{dt} = k_{l1} \times Central - Liver[k_{l2} + k_{lex}] \tag{4.5}$$

$$\frac{d[Kidneys]}{dt} = k_{k1} \times Central - Kidneys[k_{k2} + k_{kex}] \tag{4.6}$$

$$\frac{d[Central]}{dt} = \frac{k_a \times R(t)}{Vd} + [k_{c2} \times CNS + k_{t2} \times Tissue + k_{l2} \times Liver + k_{k2} \times Kidney] - Central[k_{c1} + k_{t1} + k_{l1} + k_{k1}] \tag{4.7}$$

### 4.2.3 *Data Considerations*

For modeling purposes, PK parameters and data were estimated from published figures by Luo et al.[76] in addition to using average values ($t_{max}$, CL/F, V/F) which carried a wide deviation in the sample size of 24 healthy volunteers. This added additional complexity making it harder to match the simulated plasma compartment to the human data by varying

parameters of the CNS, liver, kidneys, and other tissue compartments. Additional sources of complexity were the choice of bioavailability which has an impact on the amount of drug that is absorbed from the gastrointestinal tract into the central plasma compartment. Since the absolute bioavailability of febuxostat is not known, estimates for its bioavailability vary within the literature[77,146].

### 4.2.4 *Physiologic Modeling Considerations*

Drug absorption from the gastrointestinal tract into the central plasma compartment was removed once peak concentration times were reached for both the 40mg and 80mg doses. Physiologically, it is unrealistic for the liver, kidneys, CNS, and other tissue compartments to be actively engaged in drug transport, retention, metabolism, and excretion at early time points, but it is not known how long of a delay should be applied computationally before these compartments are considered active. With the assumption that febuxostat can be retained in tissues it is not known how long they are retained for and the rate of release from these tissues back into the central compartment, where it can be broken down and removed from the body.

### 4.2.5 *Modeling Cases*

Under various cases PK parameters are varied for the CNS, tissues, liver, and kidneys compartments that would produce a simulated plasma compartment which could be compared to human plasma data for the 40 and 80mg cases from Luo et al.[76]. Initial guesses are used as inputs for MATLAB 2017b and through least squares optimization, rate constants for the CNS, tissue, liver, and kidney compartments are varied to minimize the difference (sum of squares) between the simulated plasma compartment concentration and the human

plasma compartment data. The area under the curve (AUC) is computed for the simulated plasma ($AUC_{sim}$) compartment using the trapezoidal method that can then be compared to the AUC for the published human plasma data ($AUC_{pub}$).

Four modeling cases are considered for the 40 and 80mg doses:

*Case 1: Drug movement to all compartments*

Under case 1, the hypothesis was that metabolism of drug is primarily in the liver compartment while metabolism in the CNS and tissue compartments and excretion in the kidney compartment were similar and less significant. The parameter rates entering ($k_{c1}$) and exiting ($k_{c2}$) the CNS compartment were the same, rates entering ($k_{t1}$) and exiting ($k_{t2}$) the tissue compartment were the same, rates entering ($k_{l1}$) and exiting ($k_{l2}$) the liver compartment were the same, and rate entering ($k_{k1}$) and exiting ($k_{k2}$) the kidney compartment were the same. Parameter rates for the liver were the highest, followed by the kidney, tissue, and CNS compartments.

*Case 2: No passage of febuxostat into the central nervous system*

Under case 2, the hypothesis set rates entering ($k_{c1}$) and exiting ($k_{c2}$) the CNS to zero while metabolism within the CNS was allowed to vary. Parameter rates for the liver and kidney compartments were held the same as in case 1. Parameter rates of entry, exit, and metabolism in the tissue compartment were allowed to vary. The rate of metabolism in the liver compartment held the same value as in case 1.

*Case 3: Febuxostat metabolism and excretion occurs only in liver and kidneys*

Under case 3, the hypothesis assumed no metabolism within the CNS and tissue compartments ($k_{cex}$=$k_{tex}$=0) and the rates into these compartments($k_{c1}$ & $k_{t1}$) were slower than the rates out ($k_{c2}$ & $k_{t2}$). The remaining parameter rates in the liver and kidney compartments

were allowed to vary.

*Case 4: Disease state in central nervous system with increased CNS permeability*

Under case 4, the hypothesis assumed the CNS was more permeable under a disease state. Rates entering ($k_{c1}$) and exiting ($k_{c2}$) the CNS compartment were increased but the metabolism rate was assumed to be negligible. Rates entering ($k_{l1}$) and exiting ($k_{l2}$) the liver compartment were set equal to each other and rate entering ($k_{k1}$) and exiting ($k_{k2}$) the kidney compartment were set equal to each other. The rate of metabolism in the liver compartment ($k_{lex}$) was set higher than the tissue compartment ($k_{tex}$) and higher than the rate of excretion from the kidney compartment ($k_{kex}$).

### 4.2.6 *Sensitivity Analysis for Bioavailability*

In addition to the four hypothesis-driven cases a sensitivity analysis for bioavailability is completed, using case 1 initial input PK parameters, to determine the impact bioavailability on the resulting plasma profile and optimized parameters. Bioavailability values of 70% and 90% are used as inputs to test the model sensitivity.

## 4.3 Results

### 4.3.1 *Case 1: Drug Movement to All Compartments*

The simulated plasma concentration profiles (Figure 4.2) captured the drug profiles of the published human plasma data even though the peak concentrations for the 40mg dose (1013 ng/mL) and 80mg dose (1648 ng/mL) were slightly smaller than the published values. After optimization for the 40mg dose (Table 4.2), the CNS, tissue, and liver compartments returned

the same best-fit rate value of 0.0081 $hr^{-1}$ entering and exiting each compartment. The kidney compartment had the best-fit rate value of 0.126 $hr^{-1}$ entering ($k_{k1}$) and exiting ($k_{k2}$) compartment. Best-fit metabolism rates were the same for both the CNS and tissue compartments ($k_{cex} = k_{tex} = 0.242\ hr^{-1}$) while the best-fit liver metabolism and kidney excretion rates were 0.315 $hr^{-1}$ and 0.231 $hr^{-1}$ respectively.

For the 80mg dose the optimized tissue compartment parameters resulted in a lower exiting ($k_{t2}$) rate than entering ($k_{t1}$). The optimized metabolism rate of the CNS (0.242 $hr^{-1}$) yielded a higher value than the tissue metabolism (0.22 $hr^{-1}$) while the excretion rate from the kidney compartment was set at the same rate as the CNS (0.242 $hr^{-1}$) with liver metabolism set at 0.3152 $hr^{-1}$.

The rate of elimination from the plasma compartment for the 40 and 80mg simulated doses were optimized but not high enough to exactly match the human data. The human plasma compartment ($AUC_{pub}$) for both the 40 and 80mg doses were 5446.40 and 11026.95 (ng*hr/mL). The simulated plasma compartment ($AUC_{sim}$) were calculated at 5677.13 and 11061.91 (ng*hr/mL) for the 40 and 80mg doses respectively (Table 4.2). The results were good with 4.24% and 0.32% error between the simulated AUC ($AUC_{sim}$) and published human plasma data ($AUC_{pub}$) for the 40 and 80mg doses respectively.

An increase from the 40mg to 80mg dosage resulted in (1) a reduction in gastrointestinal absorption into the central plasma compartment, (2) a decrease in both tissue metabolism and the return rate from the tissue back into the plasma compartment, (3) a decrease in rates entering and exiting the liver and kidney compartments, and (4) an increase in the kidney excretion rate.

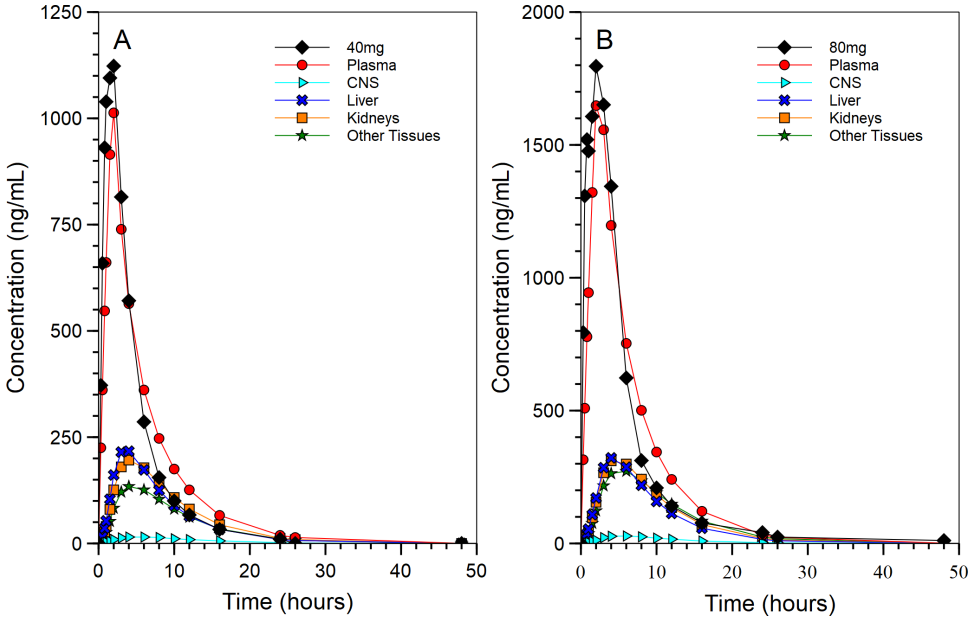


Figure 4.2: Case 1 for (A) 40mg and (B) 80mg dosing matching simulated plasma compartment to human data.

Table 4.2: Case 1: pharmacokinetic parameters used to minimize the simulated plasma compartment to published human data.

| Dose | CNS[a] | Tissues[a] | Liver[a] | Kidneys[a] | Additional |
|---|---|---|---|---|---|
| 40mg | $k_{c1}$=0.0081<br>$k_{c2}$=0.0081<br>$k_{cex}$=0.2420 | $k_{t1}$=0.0810<br>$k_{t2}$=0.0810<br>$k_{tex}$=0.2420 | $k_{l1}$=0.1800<br>$k_{l2}$=0.1800<br>$k_{lex}$=0.3150 | $k_{k1}$=0.1260<br>$k_{k2}$=0.1260<br>$k_{kex}$=0.2310 | $k_a$=1.34[b]<br>$AUC_{pub}$=5446.40[b]<br>$AUC_{sim}$=5677.13 |
| 80mg | $k_{c1}$=0.0081<br>$k_{c2}$=0.0081<br>$k_{cex}$=0.2420 | $k_{t1}$=0.0810<br>$k_{t2}$=0.0450<br>$k_{tex}$=0.2200 | $k_{l1}$=0.1260<br>$k_{l2}$=0.1260<br>$k_{lex}$=0.3152 | $k_{k1}$=0.1080<br>$k_{k2}$=0.1080<br>$k_{kex}$=0.2420 | $k_a$=1.10[b]<br>$AUC_{pub}$=11026.95[b]<br>$AUC_{sim}$=11061.91 |

[a] fitted parameters ($hr^{-1}$)
[b] calculated from Luo et al.[76]

### 4.3.2 *Case 2: No Passage of Febuxostat into Central Nervous System*

The simulated plasma concentration profiles, after optimization (best-fit) (Table 4.3), deviated slightly from the human plasma data (Figure 4.3) for both doses. Under the 40mg dose the concentration peaked at 1013 ng/mL and under the 80mg dose the concentration peaked at 1648 ng/mL. For both the 40 and 80mg doses the rates entering and exiting the liver and kidney compartments remained the same as in case 1 while the kidney excretion rate increased for the 40mg dose in case 2 (0.2970 $hr^{-1}$) compared to case 1 (0.2310 $hr^{-1}$) to help counteract the decreased metabolism rate in the system when the rate entering the CNS compartment is set to zero. When the entry, exit, and metabolism rates of the tissue compartment were allowed to vary, for the 40mg dose, the metabolism rate increased between case 1 (0.2420 $hr^{-1}$) and case 2 (0.2970 $hr^{-1}$). The rate entering the tissue compartment also increased when the rate entering the CNS compartment was set to zero.

Increasing the dose to 80mg in case 2, the rates entering and exiting the liver and kidney compartments decreased in addition to a decrease in the exiting rate from the tissue compartment. The metabolism rate of the tissue compartment decreased while there was a slight increase in the liver compartment. The Kidney excretion rate also decreased compared to the 40mg dose. When compared to case 1 for the 80mg dose, the tissue compartment increased its metabolism rate to counteract the loss of entry to the CNS compartment.

The simulated plasma compartment $AUC_{sim}$ for both doses were predicted at 5469.92 and 11107.20 (ng*hr/mL) for the 40 and 80mg doses respectively (Table 4.3). This deviates by 0.43% and 0.73% from the published human plasma data ($AUC_{pub}$) for the 40 and 80mg doses respectively.

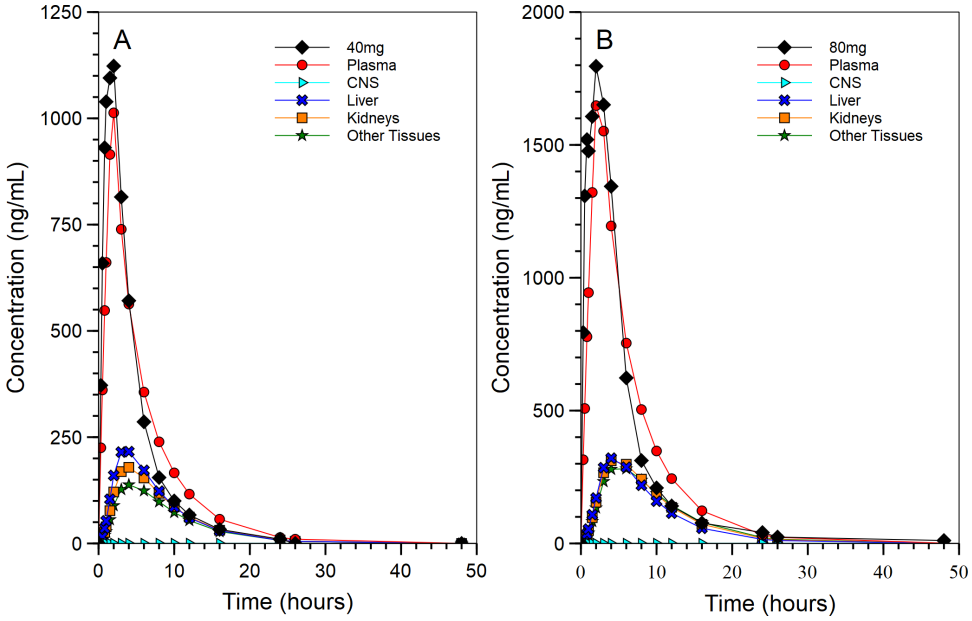


Figure 4.3: Case 2 for 40mg and 80mg assuming not passage of febuxostat into the central nervous system.

Table 4.3: Case 2: pharmacokinetic parameters assuming no central nervous system involvement ($k_{c1} = k_{c2} = k_{cex} = 0$).

| Dose | CNS | Tissues[a] | Liver[a] | Kidneys[a] | Additional |
|---|---|---|---|---|---|
| 40mg | $k_{c1}$=0.0000<br>$k_{c2}$=0.0000<br>$k_{cex}$=0.0000 | $k_{t1}$=0.0900<br>$k_{t2}$=0.0810<br>$k_{tex}$=0.2970 | $k_{l1}$=0.1800<br>$k_{l2}$=0.1800<br>$k_{lex}$=0.3150 | $k_{k1}$=0.1260<br>$k_{k2}$=0.1260<br>$k_{kex}$=0.2970 | $k_a$=1.34[b]<br>$AUC_{pub}$=5446.40[b]<br>$AUC_{sim}$=5469.92 |
| 80mg | $k_{c1}$=0.0000<br>$k_{c2}$=0.0000<br>$k_{cex}$=0.0000 | $k_{t1}$=0.0900<br>$k_{t2}$=0.0540<br>$k_{tex}$=0.2420 | $k_{l1}$=0.1260<br>$k_{l2}$=0.1260<br>$k_{lex}$=0.3154 | $k_{k1}$=0.1080<br>$k_{k2}$=0.1080<br>$k_{kex}$=0.2420 | $k_a$=1.10[b]<br>$AUC_{pub}$=11026.95[b]<br>$AUC_{sim}$=11107.20 |

[a] fitted parameters ($hr^{-1}$)
[b] calculated from Luo et al.[76]

### 4.3.3 *Case 3: Febuxostat Metabolism and Excretion Occurs Only in Liver and Kidneys*

Under the assumption that metabolism does not occur in the tissues and CNS the simulated plasma compartment (Figure 4.4) reached a lower peak concentration in both 40mg (950 ng/mL) and 80mg (1476 ng/mL) doses that was lower than what was seen in case 1 and case 2.

For both the 40and 80mg doses when no metabolism rate is assumed for the CNS and tissue compartments, higher rates exiting the tissue, CNS, and kidney compartments back to the central compartment occurred. The liver compartment rates entering and exiting remained the same for the 40 and 80mg doses (Table 4.4). To compensate for higher rates back into the central compartment the kidney and liver compartments increased their rate of metabolism and excretion respectively with the 40mg dose showing higher rates than the 80mg dose. While case 3 also showed a reduction in metabolism and excretion rates for the liver (0.4234 $hr^{-1}$ to 0.333 $hr^{-1}$) and kidney (0.3520 $hr^{-1}$ to 0.2750 $hr^{-1}$) compartments, increasing from the 40mg to 80mg doses, these rates were higher than both cases 1 and 2 at both doses.

The simulated plasma compartment $AUC_{sim}$ for both doses were calculated at 5526.20 and 10802.09 (ng*hr/mL) for the 40 and 80mg doses respectively (Table 4.4). This deviates by 1.47% and 2.04% from the published human plasma data ($AUC_{pub}$) for the 40 and 80mg doses respectively.

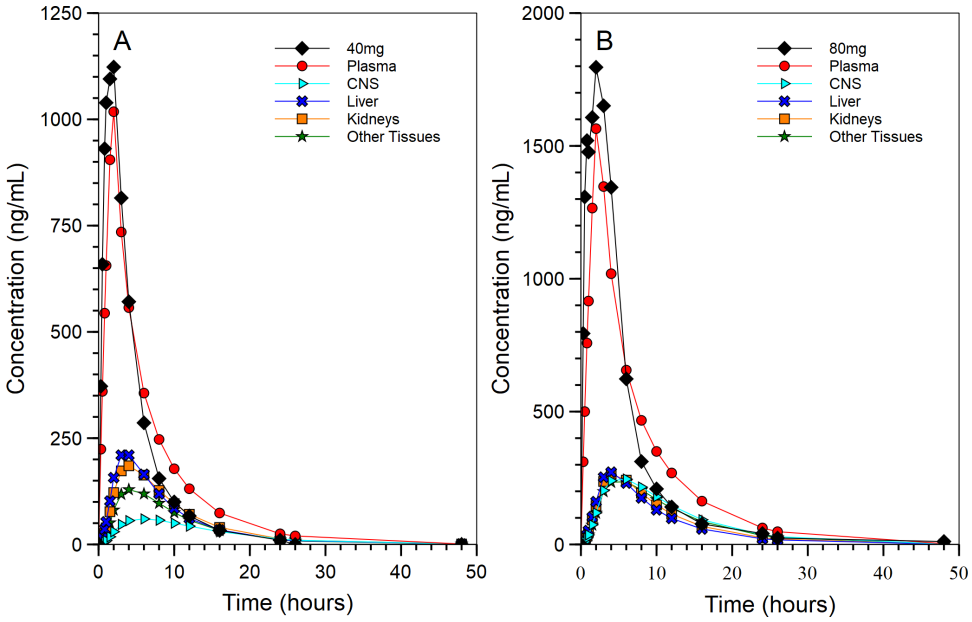


Figure 4.4: Case 3 for 40mg and 80mg assuming metabolism only occurs in the liver and kidneys.

Table 4.4: Case 3: pharmacokinetic parameters assuming no metabolism within CNS and tissue compartments ($k_{cex} = k_{tex} = 0$).

| Dose | CNS[a] | Tissues[a] | Liver[a] | Kidneys[a] | Additional |
|---|---|---|---|---|---|
| 40mg | $k_{c1}$=0.0081<br>$k_{c2}$=0.1646<br>$k_{cex}$=0.0000[b] | $k_{t1}$=0.0810<br>$k_{t2}$=0.3295<br>$k_{tex}$=0.0000[b] | $k_{l1}$=0.2702<br>$k_{l2}$=0.2700<br>$k_{lex}$=0.4234 | $k_{k1}$=0.1801<br>$k_{k2}$=0.2110<br>$k_{kex}$=0.3520 | $k_a$=1.34[c]<br>$AUC_{pub}$=5446.40[c]<br>$AUC_{sim}$=5526.20 |
| 80mg | $k_{c1}$=0.0081<br>$k_{c2}$=0.0810<br>$k_{cex}$=0.0000[b] | $k_{t1}$=0.0810<br>$k_{t2}$=0.2860<br>$k_{tex}$=0.0000[b] | $k_{l1}$=0.2340<br>$k_{l2}$=0.2340<br>$k_{lex}$=0.3330 | $k_{k1}$=0.1800<br>$k_{k2}$=0.2420<br>$k_{kex}$=0.2750 | $k_a$=1.10[c]<br>$AUC_{pub}$=11026.95[c]<br>$AUC_{sim}$=10802.09 |

[a] fitted parameters ($hr^{-1}$)
[b] assumed parameters ($hr^{-1}$)
[c] calculated from Luo et al.[76]

### 4.3.4 *Case 4: Disease State in Central Nervous System with Increased CNS Permeability*

Under the assumption that permeability is increased (Figure 4.5) in the CNS, the rate into the CNS was increased by more than double (0.0270 $hr^{-1}$, Table 4.5) compared to cases 1 and 3 (0.0081 $hr^{-1}$) for the 40mg dose. CNS entry rates increased by approximately ten-fold (0.0841 $hr^{-1}$) compared to case 1 and 3 (0.0081 $hr^{-1}$) for the 80mg dose after best-fit optimization. The rate exiting the CNS for case 4 approximately doubled between the 40mg (0.1350 $hr^{-1}$) and 80mg (0.2571 $hr^{-1}$) doses compared to case 1 where the rate exiting the compartment remained the same and case 3 where the rate exiting the CNS into the central compartment was cut approximately in half when increasing from the 40 to 80mg dose. Peak concentration levels were higher for both the 40mg (1018 ng/mL) and 80mg (1565 ng/mL) doses than those seen in case 3.

The simulated plasma compartment $AUC_{sim}$ for both doses were calculated at 5471.20 and 11051.53 (ng*hr/mL) for the 40 and 80mg doses respectively (Table 4.5). This deviates by 0.46% and 0.22% from the published human plasma data ($AUC_{pub}$) for the 40 and 80mg doses respectively.

Table 4.5: Case 4: pharmacokinetic parameters for central nervous system disease state ($k_{cex} = 0$).

| Dose | CNS[a] | Tissues[a] | Liver[a] | Kidneys[a] | Additional |
|---|---|---|---|---|---|
| 40mg | $k_{c1}$=0.0270<br>$k_{c2}$=0.1350<br>$k_{cex}$=0.0000[b] | $k_{t1}$=0.0810<br>$k_{t2}$=0.0810<br>$k_{tex}$=0.2750 | $k_{l1}$=0.1800<br>$k_{l2}$=0.1800<br>$k_{lex}$=0.3600 | $k_{k1}$=0.1260<br>$k_{k2}$=0.1260<br>$k_{kex}$=0.2750 | $k_a$=1.34[c]<br>$AUC_{pub}$=5446.40[c]<br>$AUC_{sim}$=5471.20 |
| 80mg | $k_{c1}$=0.0814<br>$k_{c2}$=0.2571<br>$k_{cex}$=0.0000[b] | $k_{t1}$=0.0810<br>$k_{t2}$=0.0511<br>$k_{tex}$=0.2205 | $k_{l1}$=0.1263<br>$k_{l2}$=0.1356<br>$k_{lex}$=0.3487 | $k_{k1}$=0.1083<br>$k_{k2}$=0.1230<br>$k_{kex}$=0.2640 | $k_a$=1.10[c]<br>$AUC_{pub}$=11026.95[c]<br>$AUC_{sim}$=11051.53 |

[a] fitted parameters ($hr^{-1}$)
[b] assumed parameters ($hr^{-1}$)
[c] calculated from Luo et al.[76]

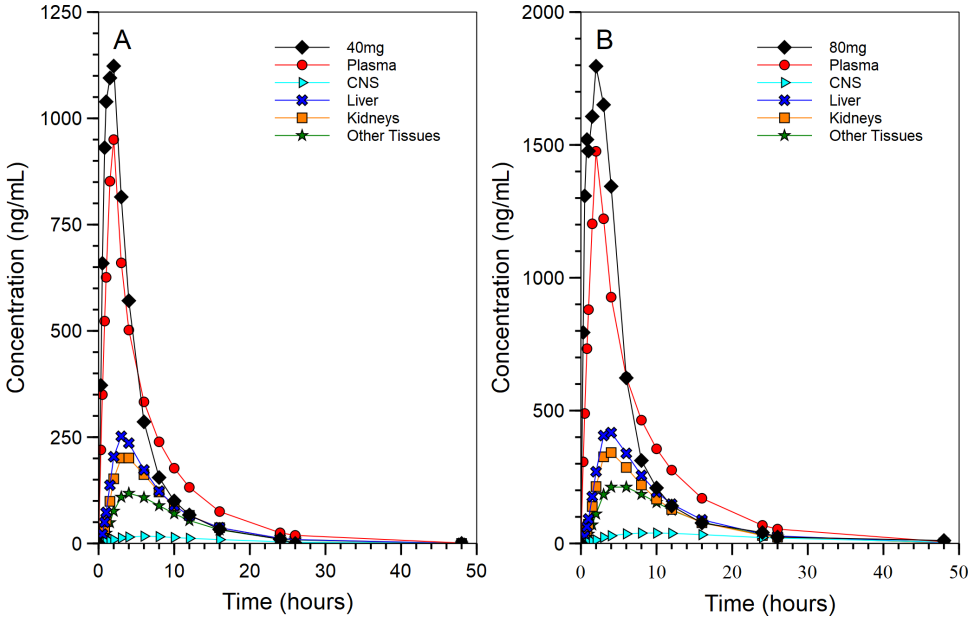


Figure 4.5: Case 4 assuming for 40mg and 80mg assuming increased CNS permeability.

### 4.3.5 *Sensitivity Analysis for Bioavailability*

Visual inspection of the 40mg (Figure 4.6) and 80mg (Figure 4.7) dose shows that bioavailability has an increased effect on the steepness of absorption into the plasma compartment when varied at 70, 80, and 90%. Sensitivity analysis for the 40mg (Table 4.6) dose reveals no changes in CNS, liver, kidney, or other tissue compartment PK parameters with the bioavailability input of 70 and 80%, but the $AUC_{sim}$ for the 70% input is lower than for the 80% input resulting in a percent error increase from 4.24% (80% bioavailability) to 9.30% (70% bioavailability). When the bioavailability is increased from 80% to 90% the PK parameter rate for CNS entry into the CNS increases and the rates for entering, exiting, and metabolism in the liver also increase. This change leads to an $AUC_{sim}$ of 5862.18 and a percent error of 7.63% from the human plasma compartment data. For the 80mg dose (Table 4.7) the 70% bioavailability input resulted in increased exiting rates from all peripheral compartments back to the central plasma compartment with reductions in metabolism/excretion from the CNS, liver, and kidneys compared to the 80% bioavailability. When the bioavailability is

increased further to 90% only metabolism in the liver compartment increases in addition to increased rates of entry into the CNS. AUC percent error, comparing simulations ($AUC_{sim}$) to human plasma data ($AUC_{pub}$), for the 70% (10.53%) input decreases to 0.32% when 80% bioavailability is reached but then increases to 1.50% when bioavailability is increased further to 90% for the 80mg dose.

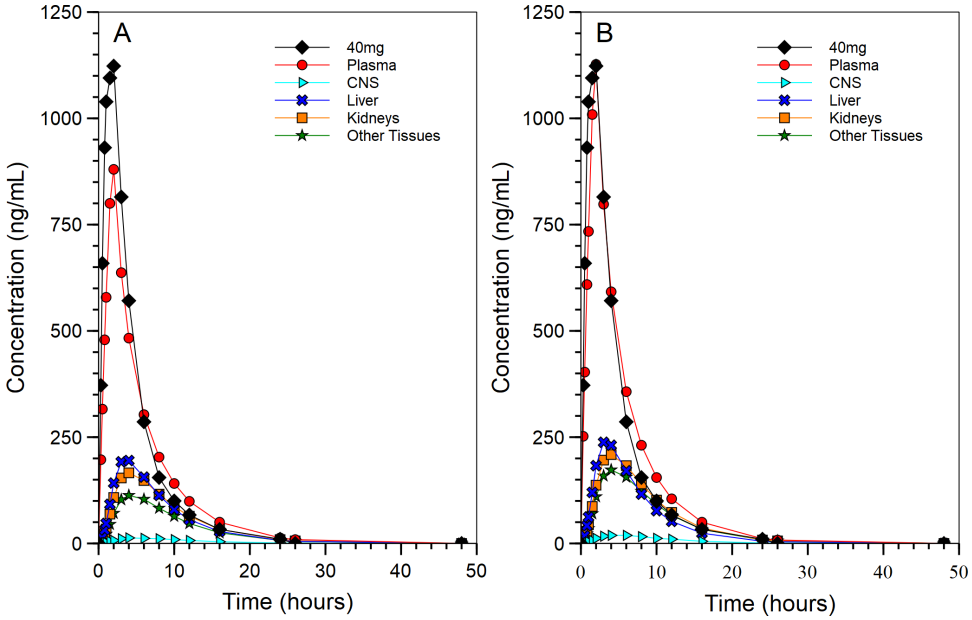


Figure 4.6: Sensitivity analysis using (A) 70% and (B) 90% bioavailability for 40mg dose. Compartment profiles for 80% bioavailability can be found in Figure 4.2(A).

## 4.4 Discussion and Conclusions

### 4.4.1 *Case Considerations*

A total of 4 hypothesis-based cases were presented where PK parameters were varied within different compartments with the goal of simulating a plasma compartment similar to human published data. This approach could help provide insight into potential PK values for each compartment. As parameters were varied to minimize error between the human and

Table 4.6: Pharmacokinetic parameters resulting from sensitivity analysis for 40mg dose at 70, 80, and 90% bioavailability.

| Bioavailability (%) | CNS[a] | Tissues[a] | Liver[a] | Kidneys[a] | Additional |
|---|---|---|---|---|---|
| 70 | $k_{c1}$=0.0081<br>$k_{c2}$=0.0081<br>$k_{cex}$=0.2420 | $k_{t1}$=0.0810<br>$k_{t2}$=0.0810<br>$k_{tex}$=0.2420 | $k_{l1}$=0.1800<br>$k_{l2}$=0.1800<br>$k_{lex}$=0.3150 | $k_{k1}$=0.1260<br>$k_{k2}$=0.1260<br>$k_{kex}$=0.2310 | $k_a$=1.34[b]<br>$AUC_{pub}$=5446.40[b]<br>$AUC_{sim}$=4939.69 |
| 80 | $k_{c1}$=0.0081<br>$k_{c2}$=0.0081<br>$k_{cex}$=0.2420 | $k_{t1}$=0.0810<br>$k_{t2}$=0.0810<br>$k_{tex}$=0.2420 | $k_{l1}$=0.1800<br>$k_{l2}$=0.1800<br>$k_{lex}$=0.3150 | $k_{k1}$=0.1260<br>$k_{k2}$=0.1260<br>$k_{kex}$=0.2310 | $k_a$=1.34[b]<br>$AUC_{pub}$=5446.40[b]<br>$AUC_{sim}$=5677.13 |
| 90 | $k_{c1}$=0.0099<br>$k_{c2}$=0.0081<br>$k_{cex}$=0.2420 | $k_{t1}$=0.0990<br>$k_{t2}$=0.0810<br>$k_{tex}$=0.2420 | $k_{l1}$=0.1924<br>$k_{l2}$=0.2001<br>$k_{lex}$=0.3850 | $k_{k1}$=0.1260<br>$k_{k2}$=0.1260<br>$k_{kex}$=0.2310 | $k_a$=1.34[b]<br>$AUC_{pub}$=5446.40[b]<br>$AUC_{sim}$=5862.18 |

[a] fitted parameters ($hr^{-1}$)
[b] calculated from Luo et al.[76]

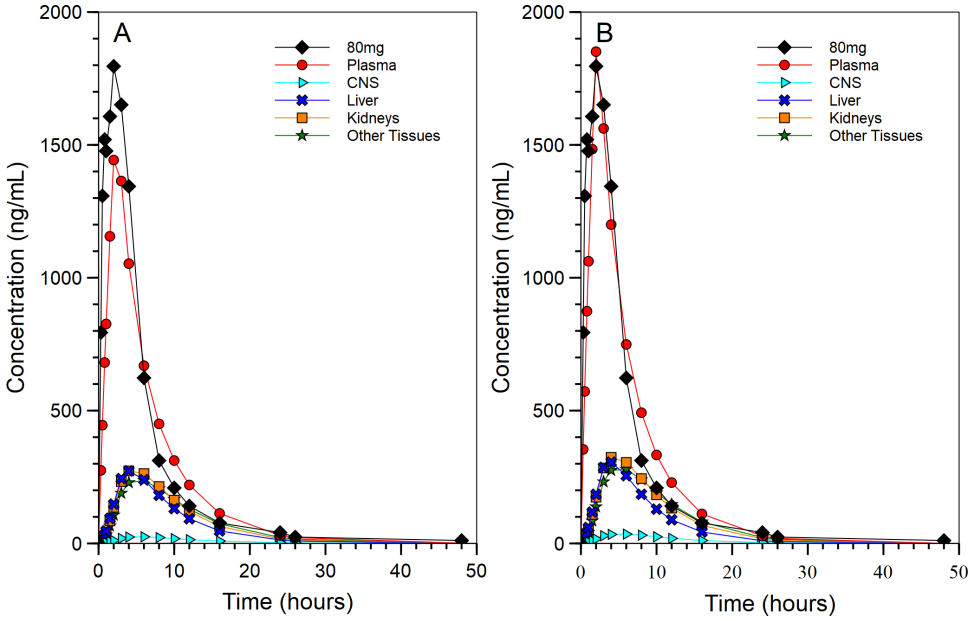


Figure 4.7: Sensitivity analysis using (A) 70% and (B) 90% bioavailability for 80mg dose. Compartment profiles for 80% bioavailability can be found in Figure 4.2(B).

Table 4.7: Pharmacokinetic parameters resulting from sensitivity analysis for 80mg dose at 70, 80, and 90% bioavailability.

| Bioavailability (%) | CNS[a] | Tissues[a] | Liver[a] | Kidneys[a] | Additional |
|---|---|---|---|---|---|
| 70 | $k_{c1}$=0.0081<br>$k_{c2}$=0.009<br>$k_{cex}$=0.2382 | $k_{t1}$=0.0811<br>$k_{t2}$=0.0501<br>$k_{tex}$=0.2200 | $k_{l1}$=0.1263<br>$k_{l2}$=0.1336<br>$k_{lex}$=0.3356 | $k_{k1}$=0.1083<br>$k_{k2}$=0.1212<br>$k_{kex}$=0.2302 | $k_a$=1.10[b]<br>$AUC_{pub}$=11026.95[b]<br>$AUC_{sim}$=9865.96 |
| 80 | $k_{c1}$=0.0081<br>$k_{c2}$=0.0081<br>$k_{cex}$=0.2420 | $k_{t1}$=0.0810<br>$k_{t2}$=0.0450<br>$k_{tex}$=0.2200 | $k_{l1}$=0.1260<br>$k_{l2}$=0.1260<br>$k_{lex}$=0.3152 | $k_{k1}$=0.1080<br>$k_{k2}$=0.1080<br>$k_{kex}$=0.2420 | $k_a$=1.10[b]<br>$AUC_{pub}$=11026.95[b]<br>$AUC_{sim}$=11061.91 |
| 90 | $k_{c1}$=0.0099<br>$k_{c2}$=0.0081<br>$k_{cex}$=0.2420 | $k_{t1}$=0.0810<br>$k_{t2}$=0.0450<br>$k_{tex}$=0.2200 | $k_{l1}$=0.1260<br>$k_{l2}$=0.1260<br>$k_{lex}$=0.3831 | $k_{k1}$=0.1080<br>$k_{k2}$=0.1080<br>$k_{kex}$=0.2420 | $k_a$=1.10[b]<br>$AUC_{pub}$=11026.95[b]<br>$AUC_{sim}$=11192.41 |

[a] fitted parameters ($hr^{-1}$)
[b] calculated from Luo et al.[76]

simulated plasma compartments some unlikely results emerged. For cases 1 and 2 the rate of entry into the peripheral compartments and rates of return to the central plasma compartment were either equal to each other or the rate of return to the central compartment was lower than the rate of entry into the peripheral compartments. Cases 3 and 4 resulted in higher rates exiting the peripheral compartments than entry into the compartments from the central plasma compartment.

Plausibility of the computational models would need to be reinforced by both *in vitro* and *in vivo* experiments with febuxostat in both healthy and diseased states to understand both transport mechanisms as well as cell and tissue uptake in both states. Normally the BBB is highly selective and restricts the movement of compounds into the CNS but under disease states such as MS, Alzheimer's, and ASD permeability can increase resulting in drug movement into the CNS but those levels are unknown.

Cases 1, 3, and 4 generated CNS concentration profiles where case 1 parameters are optimized to low rates of entry and exit from the CNS while also assuming metabolism within the compartment. Cases 3 and 4 produced higher rates of entry and exit from the CNS while

also assuming no metabolism within the compartment. Out of these three cases, case 1 appears to be more plausible as it allows for metabolism even though the entry and exit rates are low. Case 2 assumes zero rates of entry, exit, and metabolism ($k_{c1} = k_{c2} = k_{cex} = 0$) making it less plausible than case 1 since brain tissue has the potential to metabolize febuxostat by P450 enzymes. Currently there is no published literature on febuxostat that would give insight into the potential for metabolism by other tissues such as fat and muscle. Due to the lack available information on this topic multiple tissue types were lumped together resulting a single tissue compartment. While assumptions about compartments were made, case 1 would still make a good candidate model as it includes metabolism/excretion from the liver, kidneys, and CNS compartments which cases 2-4 do not have. With case 1 being identified as the most plausible prediction model from this study it would next need to be tested and validated on its ability to accurately predict a new set of human PK data.

A major drawback of human multi-compartment PK models, in general, is the lack of biological data. It is not feasible to obtain and process human organs at various time points to track drug absorption, distribution, and metabolism useful for modeling. At best, animal models can be used as a substitute but an appropriate model must be chosen with anatomy and physiology which closely matches humans. Through computational modeling we were able to simulate drug flow into various compartments, with and without restrictions, to determine models which may give some insight into drug distribution scenarios that would reproduce the plasma concentration profile from Luo et al.[76]. The strength of the case 1 model is its ability to be adapted and expanded on as future data and studies surrounding febuxostat absorption, distribution, metabolism, and excretion becomes available in the future, but for now it is a good start.

Potential uses for this model would include studying febuxostat distribution into the CNS in patients with pre-existing neurodegenerative disorders such as ASD, MS, and Alzheimer's

that may encounter gout episodes in their lifetime when the BBB in these patient populations is compromised. Having an understanding of the amount of drug that could cross into the CNS using approved doses (40 and 80mg) of febuxostat as well as drug metabolism in the CNS can lead to treatment modifications in patients with a compromised BBB to minimize potential drug side effects.

Future modeling approaches can investigate the impact of the remaining tissues on drug distribution as various tissue types may retain febuxostat for different amounts of time which would impact the rate of return to the central compartment. The number of compartments can either be reduced or increased once this information is known to generate a better model. Future approaches can also look into drug-protein binding in the blood which will affect the distribution of febuxostat throughout the body due to its increase in size when bound to proteins.

## 4.5 Acknowledgments

We would like to thank Mr. Richard Yea and Ms. Morgan Haywood for their assistance as well as Virginia Tech Initiative for Maximizing Student Development (VT-IMSD).

# Chapter 5

# Conclusions and Future Directions

Elevated blood levels of XO and brain oxidative stress have been documented in human ASD patients compared to non-ASD patients with no known cause. Preliminary research from the Lee lab group has documented elevated mRNA expression levels of XO as well as elevated oxidative stress in the brain tissue of autistic (BTBR) mice compared to control (C57) mice. The purpose of this project was to (1) investigate if a reduction of oxidative stress in the brain tissue of BTBR mice would lead to cognitive improvements, and (2) develop two computational models to predict transport to the brain. This lead to the development of the three specific aims below. For this project, febuxostat was chosen as the drug candidate of study for its lipophilicity, ability to inhibit XO, and its higher potency and better renal clearance compared to allopurinol.

**Aim 1:** Model the transport of lipophilic compounds across a BBB mimic.

**Aim 2:** Determine if XO-inhibition lowers oxidative stress resulting in cognitive improvement.

**Aim 3:** Create a pharmacokinetic multi-compartment model to study the body distribution and penetration of febuxostat into the CNS and brain tissue.

## 5.1 Specific Aim 1: Conclusions, Relevance, Limitations

In the first study, FITC was examined as a candidate for passive diffusion across an HBMEC *in vitro* model due to its similar properties to febuxostat and its isothiocyanate chain that has been shown to diffuse into cells in the literature. Both NaFl and flourescein (unconjugated) were chosen as controls because NaFl was predicted to lack the ability to cross the cell membrane due to its lack of lipophilicity and fluorescein (unconjugated) was expected to not penetrate into the cell as it lacked the isothiocyanate chain. *In vitro* computational simulations of the three fluorescent tracers into an HBMEC model revealed that only simulations of FITC could be reproduced that resulted in data that closely matching the *in vitro* experiments. The continual increases in FITC concentration over the duration of the *in vitro* experiments lends itself to the assumption of passive diffusion. Both computational and *in vitro* results for NaFl and fluorescein showed that the assumption of passive diffusion was not suited for these tracers indicating that other models must be used to explain the fluorescent intensity that remained with the cell monolayers after multiple washes.

Relevance of this work is two-fold in that it evaluates approaches to (1) computationally determine physical parameters in an *in vitro* system and (2) demonstrates a procedure of substituting lipophilic drug of interests with fluorescent compounds allowing for detection of low concentrations. These approaches can be used as alternatives to more costly and time-consuming methods of determining concentrations of compounds within cells and diffusion constants.

Although the signal was low we were able to show and quantify that FITC could be modeled by passive diffusion but a few limitations need to be addressed within the study that need improvement. First, the signal read from cell cultures plates gave no indication of where

tracers were contained. This made it hard to distinguish between tracer that may have been within the cell cytoplasm, stuck in the plasma membrane, or remained bound at the surface after multiple washes. The approach of using fluorescent readings allowed for detection of small amounts of tracer, but the drawback was that the location of tracer remained unknown. Calculations of tracer amounts were also based on the expected volume within each well when converting from fluorescent units to mass. Since volume amounts were estimated based on assumed monolayer heights of 1 µm and 5 µm the resulting tracer mass calculations could vary from what was reported if the cell heights were under or over estimated. Monolayer heights of 1 µm and 5 µm where chosen as they were within the range of normal cells (1 to 10 µm), but the exact height of the monolayers was unable to be determined experimentally. Also while computational simulations could give information about depth of tracer amounts, based on effective diffusion constants ($D_{eff}$), this could not be validated by *in vitro* methods that only gave aggregate information such as total fluorescent intensity for each well. Once these limitations are addressed a better experimental protocol can be developed that would help validate computational simulations.

## 5.2 Specific Aim 2: Conclusions, Relevance, Limitations

In this study, on the effects of febuxostat on behavior and oxidative stress, no statistically significant differences were found between the BTBR vehicle group (5% v/v DMSO in PBS) and BTBR treatment groups (vehicle + 10mg/kg febuxostat) after seven days of once daily dosing by I.P injection in male juvenile mice. Three questions remained at the conclusion of this study, (1) were the BTBR mice exposed to febuxostat systemically from IP injection, (2) if systemic exposure occurred did febuxostat reach the brain tissue, and (3) was the chosen

dose and treatment schedule appropriate to see any changes in behavior and oxidative stress? As there are no other published studies on behavioral changes and reductions of oxidative stress in a BTBR model using febuxostat a dose of 10mg/kg per day may have been too low to have any effect, assuming febuxostat was absorbed into the blood and reached the brain.

To address these questions multiple approaches can be used such as (1) a dose escalation study with I.P injections and (2) direct delivery to the brain with escalating doses. In a dose escalation study each successive cohort of mice, receiving febuxostat treatment, would be exposed to higher doses until negative effects emerge due to either toxicity or sedative effects. With direct delivery the BBB is bypassed and febuxostat can be exposed directly to the brain that would require a dose escalation study as well. Once a safe dosing range is found the behavioral and oxidative stress experiments could be repeated with the C57 and BTBR groups to determine if there are any behavioral changes and reductions of oxidative stress in BTBR mice treated with febuxostat.

After these tests are repeated, following studies on dose and delivery methods, the relevance of using febuxostat can be better evaluated. Currently some limitations do exist with the study related to the use of brain tissue and the detection of oxidative stress. In the study brain tissues were frozen and stored until time was available for processing; this could result in loss of oxidative stress detection especially if tissues are stored for long periods of time. To address this, tissues should be processed as quickly as possible to have the best response using the DHE stain. Also due to the small size of the juvenile mouse brain entire sections, along sagittal plane, were used. To help with better comparison between treatment groups specific brain regions can be identified for sectioning and a rodent brain matrix can be used to create reproducible sectioning.

## 5.3 Specific Aim 3: Conclusions, Relevance, Limitations

In the third study four hypothesis-based PK models were proposed and evaluated for their ability to describe the absorption, distribution, metabolism, and excretion of febuxostat in the central plasma, CNS, liver, kidneys, and remaining tissue compartments. Sensitivity analysis was carried out on a bioavailability range from 70-90% to evaluate how modeling parameters changed as the plasma concentration profile was varied. Out of all models, case 1 was selected as the most plausible of the four as the brain has the capacity for drug metabolism if substances can cross into the CNS which is possible in diseases where BBB disruption and dysfunction have been documented. Case 1 was also chosen as the optimization (best-fit) parameters resulted in rates entering peripheral compartments (CNS, liver, kidneys, other tissues) that were either equal to or higher than the rates leaving these compartments, returning to the central plasma compartment.

Currently there are no published multi-compartment PK models for febuxostat, which would make the model from our study a good starting point that can be re-evaluated and updated as more human PK data for peripheral compartments becomes available. This study also has potential clinical relevance as it can be used to study movement of febuxostat into the CNS of patients that may have a compromised BBB which would help improve patient care. The study also allows considering other plausible hypotheses to be investigated if experimental data (*in vitro* or *in vivo*) for different compartments (i.e. tissues or organs) are generated or tracked in the future.

A few of the limitations of the third study are (1) the lack of human PK data for febuxostat in multiple tissues, (2) the method of parameter optimization, and (3) population differences. Generally in animal models both plasma and tissue samples can be taken to determine drug

concentrations, but in humans blood sampling is the primary method as tissue sampling is too invasive which limits the amount of available data for use in a multi-compartment PK model that includes tissues. For computational simulations initial PK model parameter inputs vary all compartments which would result in the simulated plasma compartment approaching values for the human plasma data it is compared to. An optimization-based parameter identification approach was employed to identify the best set of PK model parameter values. An issue with this approach is that a global optimization algorithm, such as genetic algorithm or simulated annealing, is needed. In the study a local optimization algorithm was employed, in which case the results were influenced by the initial starting parameter values. To counter this initial PK parameters need to have starting points over a wider range and the results compared to locate additional plausible optimized parameters for each compartment. Lastly, population variability needs to be considered as age, race, and gender are potential factors that would have an impact on drug metabolism in the body making it harder to apply. One potential approach to address this limitation would be to include data from as many significant sources of variability as possible to create a more robust model that can be used.

## 5.4 Future Work

Future work could involve two routes: (1) determination of a safe therapeutic dose of febuxostat that could lead to behavioral changes and a reduction of oxidative stress in autism mice and (2) the creation of a multi-compartment mouse PK model which could potentially be scaled up for humans. For the first route, discussed in section 5.2, it needs to be determined (1) if there is any safe therapeutic dose that can reduce oxidative stress in brain tissue of mice by oral administration or direct delivery of febuxostat and (2) if a reduction in oxidative stress, caused by elevated levels of XO, could lead to behavioral improvements.

This information would be needed to determine if XO-inhibition with febuxostat should be continued.

The second route for future work would shift PK modeling to a mouse model which would allow for more information to be gathered on concentrations within the blood plasma and different tissues following oral administration, distribution, metabolism ,and excretion at various doses. This animal model approach would also allow for the study of CNS permeability following BBB disruption and dysfunction to quantify the potential amounts of drug that could cross into brain tissue. Once PK parameters are calculated from the studies these can be scaled up to build a human prediction model where the predictions could be compared to available published human data for validation.

# Bibliography


[1] J. Baio, L. Wiggins, D. L. Christensen, M. J. Maenner, J. Daniels, Z. Warren, M. Kurzius-Spencer, W. Zahorodny, C. R. Rosenberg, T. White, *et al.*, "Prevalence of autism spectrum disorder among children aged 8 years—autism and developmental disabilities monitoring network, 11 sites, united states, 2014," *Morbidity and Mortality Weekly Report. Surveillance Summaries*, vol. 67, no. 6, p. 1, 2018.

[2] D. L. Christensen, J. Baio, K. Van Naarden Braun, D. Bilder, J. Charles, J. N. Constantino, J. Daniels, M. S. Durkin, R. T. Fitzgerald, M. Kurzius-Spencer, L. C. Lee, S. Pettygrove, C. Robinson, E. Schulz, C. Wells, M. S. Wingate, W. Zahorodny, and M. Yeargin-Allsopp, "Prevalence and characteristics of autism spectrum disorder among children aged 8 years–autism and developmental disabilities monitoring network, 11 sites, united states, 2012," *Morbidity and Mortality Weekly Report. Surveillance Summaries*, vol. 65, no. 3, pp. 1–23, 2016.

[3] G. Montes and J. S. Halterman, "Characteristics of school-age children with autism," *Journal of Developmental & Behavioral Pediatrics*, vol. 27, no. 5, pp. 379–85, 2006.

[4] D. C. Llaneza, S. V. DeLuke, M. Batista, J. N. Crawley, K. V. Christodulu, and C. A. Frye, "Communication, interventions, and scientific advances in autism: a commentary," *Physiology & Behavior*, vol. 100, no. 3, pp. 268–76, 2010.

[5] A. Zuddas, "Autism assessment tools in the transition from dsm-iv to dsm-5," *European Child & Adolescent Psychiatry*, vol. 22, no. 6, pp. 325–7, 2013.

[6] J. A. Christiansz, K. M. Gray, J. Taffe, and B. J. Tonge, "Autism spectrum disorder

in the dsm-5: Diagnostic sensitivity and specificity in early childhood," *Journal of Autism and Developmental Disorders*, vol. 46, no. 6, pp. 2054–63, 2016.

[7] S. L. Logan, L. Carpenter, R. S. Leslie, E. Garrett-Mayer, K. J. Hunt, J. Charles, and J. S. Nicholas, "Aberrant behaviors and co-occurring conditions as predictors of psychotropic polypharmacy among children with autism spectrum disorders," *Journal of Child and Adolescent Psychopharmacology*, vol. 25, no. 4, pp. 323–36, 2015.

[8] S. B. Mukherjee, "Autism spectrum disorders - diagnosis and management," *Indian Journal of Pediatrics*, vol. 84, no. 4, pp. 307–314, 2017.

[9] J. Horder, C. E. Wilson, M. A. Mendez, and D. G. Murphy, "Autistic traits and abnormal sensory experiences in adults," *Journal of Autism and Developmental Disorders*, vol. 44, no. 6, pp. 1461–1469, 2014.

[10] B. K. Ahmedani and R. M. Hock, "Health care access and treatment for children with co-morbid autism and psychiatric conditions," *Social Psychiatry and Psychiatric Epidemiology*, vol. 47, no. 11, pp. 1807–14, 2012.

[11] Z. Cidav, S. C. Marcus, and D. S. Mandell, "Implications of childhood autism for parental employment and earnings," *Pediatrics*, vol. 129, no. 4, pp. 617–23, 2012.

[12] T. A. Lavelle, M. C. Weinstein, J. P. Newhouse, K. Munir, K. A. Kuhlthau, and L. A. Prosser, "Economic burden of childhood autism spectrum disorders," *Pediatrics*, vol. 133, no. 3, pp. e520–9, 2014.

[13] R. Vohra, S. Madhavan, U. Sambamoorthi, and C. St Peter, "Access to services, quality of care, and family impact for children with autism, other developmental disabilities, and other mental health conditions," *Autism*, vol. 18, no. 7, pp. 815–26, 2014.

[14] E. J. Callander and D. B. Lindsay, "The impact of childhood autism spectrum disorder on parent's labour force participation: Can parents be expected to be able to re-join the labour force?," *Autism*, pp. 542–548, 2017.

[15] J. M. Fullerton, V. Totsika, R. Hain, and R. P. Hastings, "Siblings of children with life-limiting conditions: psychological adjustment and sibling relationships," *Child: Care, Health, and Development*, vol. 43, no. 3, pp. 393–400, 2017.

[16] D. Pinto, E. Delaby, D. Merico, M. Barbosa, A. Merikangas, L. Klei, B. Thiruvahindrapuram, X. Xu, R. Ziman, Z. Wang, *et al.*, "Convergence of genes and cellular pathways dysregulated in autism spectrum disorders," *American Journal of Human Genetics*, vol. 94, no. 5, pp. 677–94, 2014.

[17] T. Mbadiwe and R. M. Millis, "Epigenetics and autism," *Autism Research and Treatment*, vol. 2013, p. 826156, 2013.

[18] R. H. Haas, "Autism and mitochondrial disease," *Developmental Disabilities Research Reviews*, vol. 16, no. 2, pp. 144–53, 2010.

[19] A. Chauhan, F. Gu, M. M. Essa, J. Wegiel, K. Kaur, W. T. Brown, and V. Chauhan, "Brain region-specific deficit in mitochondrial electron transport chain complexes in children with autism," *Journal of Neurochemistry*, vol. 117, no. 2, pp. 209–20, 2011.

[20] N. S. Mohammad, J. M. Jain, K. P. Chintakindi, R. P. Singh, U. Naik, and R. R. Akella, "Aberrations in folate metabolic pathway and altered susceptibility to autism," *Psychiatric Genetics*, vol. 19, no. 4, pp. 171–6, 2009.

[21] B. Manzi, A. L. Loizzo, G. Giana, and P. Curatolo, "Autism and metabolic diseases," *Journal of Child Neurology*, vol. 23, no. 3, pp. 307–14, 2008.

[22] S. J. James, S. Melnyk, S. Jernigan, M. A. Cleves, C. H. Halsted, D. H. Wong, P. Cutler, K. Bock, M. Boris, J. J. Bradstreet, S. M. Baker, and D. W. Gaylor, "Metabolic endophenotype and related genotypes are associated with oxidative stress in children with autism," *American Journal of Medical Genetics Part B: Neuropsychiatric Genetics*, vol. 141B, no. 8, pp. 947–56, 2006.

[23] J. K. Kern and A. M. Jones, "Evidence of toxicity, oxidative stress, and neuronal insult in autism," *Journal of Toxicology and Environmental Health Part B: Critical Reviews*, vol. 9, no. 6, pp. 485–99, 2006.

[24] S. Rose, S. Melnyk, O. Pavliv, S. Bai, T. G. Nick, R. E. Frye, and S. J. James, "Evidence of oxidative damage and inflammation associated with low glutathione redox status in the autism brain," *Translational Psychiatry*, vol. 2, p. e134, 2012.

[25] F. Gu, V. Chauhan, and A. Chauhan, "Glutathione redox imbalance in brain disorders," *Current Opinion in Clinical Nutrition and Metabolic Care*, vol. 18, no. 1, pp. 89–95, 2015.

[26] F. Gu, V. Chauhan, and A. Chauhan, "Impaired synthesis and antioxidant defense of glutathione in the cerebellum of autistic subjects: alterations in the activities and protein expression of glutathione-related enzymes," *Free Radical Biology & Medicine*, vol. 65, pp. 488–96, 2013.

[27] E. M. Sajdel-Sulkowska, M. Xu, and N. Koibuchi, "Increase in cerebellar neurotrophin-3 and oxidative stress markers in autism," *Cerebellum*, vol. 8, no. 3, pp. 366–72, 2009.

[28] L. A. LeBlanc and J. M. Gillis, "Behavioral interventions for children with autism spectrum disorders," *Pediatric Clinics of North America*, vol. 59, no. 1, pp. 147–64, xi–xii, 2012.

[29] G. Dawson and K. Burner, "Behavioral interventions in children and adolescents with autism spectrum disorder: a review of recent findings," *Current Opinion in Pediatrics*, vol. 23, no. 6, pp. 616–20, 2011.

[30] J. J. Bradstreet, S. Smith, M. Baral, and D. A. Rossignol, "Biomarker-guided interventions of clinically relevant conditions associated with autism spectrum disorders and attention deficit hyperactivity disorder," *Alternative Medicine Review*, vol. 15, no. 1, pp. 15–32, 2010.

[31] S. E. Levy and S. L. Hyman, "Novel treatments for autistic spectrum disorders," *Mental Retardation and Developmental Disabilities Research Reviews*, vol. 11, no. 2, pp. 131–42, 2005.

[32] D. A. Rossignol, "Novel and emerging treatments for autism spectrum disorders: a systematic review," *Annals of Clinical Psychiatry*, vol. 21, no. 4, pp. 213–36, 2009.

[33] R. Canitano, "Mood stabilizers in children and adolescents with autism spectrum disorders," *Clinical Neuropharmacology*, vol. 38, no. 5, pp. 177–82, 2015.

[34] M. L. McPheeters, Z. Warren, N. Sathe, J. L. Bruzek, S. Krishnaswami, R. N. Jerome, and J. Veenstra-Vanderweele, "A systematic review of medical treatments for children with autism spectrum disorders," *Pediatrics*, vol. 127, no. 5, pp. e1312–21, 2011.

[35] J. L. Silverman and J. N. Crawley, "The promising trajectory of autism therapeutics discovery," *Drug Discovery Today*, vol. 19, no. 7, pp. 838–44, 2014.

[36] J. K. Kern, D. A. Geier, J. B. Adams, C. R. Garver, T. Audhya, and M. R. Geier, "A clinical trial of glutathione supplementation in autism spectrum disorders," *Medical Science Monitor*, vol. 17, no. 12, pp. CR677–82, 2011.

[37] D. S. Warner, H. Sheng, and I. Batinic-Haberle, "Oxidants, antioxidants and the ischemic brain," *Journal of Experimental Biology*, vol. 207, no. 18, pp. 3221–31, 2004.

[38] S. Love, "Oxidative stress in brain ischemia," *Brain Pathology*, vol. 9, no. 1, pp. 119–31, 1999.

[39] S. S. Zoroglu, F. Armutcu, S. Ozen, A. Gurel, E. Sivasli, O. Yetkin, and I. Meram, "Increased oxidative stress and altered activities of erythrocyte free radical scavenging enzymes in autism," *European Archives of Psychiatry and Clinical Neurosciences*, vol. 254, no. 3, pp. 143–7, 2004.

[40] J. L. Silverman, M. Yang, C. Lord, and J. N. Crawley, "Behavioural phenotyping assays for mouse models of autism," *Nature Reviews Neuroscience*, vol. 11, no. 7, pp. 490–502, 2010.

[41] C. E. Berry and J. M. Hare, "Xanthine oxidoreductase and cardiovascular disease: molecular mechanisms and pathophysiological implications," *Journal of Physiology*, vol. 555, no. 3, pp. 589–606, 2004.

[42] R. Harrison, "Structure and function of xanthine oxidoreductase: where are we now?," *Free Radical Biology & Medicine*, vol. 33, no. 6, pp. 774–97, 2002.

[43] R. Harrison, "Physiological roles of xanthine oxidoreductase," *Drug Metabolism Reviews*, vol. 36, no. 2, pp. 363–75, 2004.

[44] Y. Yokoyama, J. S. Beckman, T. K. Beckman, J. K. Wheat, T. G. Cash, B. A. Freeman, and D. A. Parks, "Circulating xanthine oxidase: potential mediator of ischemic injury," *American Journal of Physiology*, vol. 258, no. 4 Pt 1, pp. G564–70, 1990.

[45] S. Tan, R. Radi, F. Gaudier, R. A. Evans, A. Rivera, K. A. Kirk, and D. A. Parks,

"Physiologic levels of uric acid inhibit xanthine oxidase in human plasma," *Pediatric Research*, vol. 34, no. 3, pp. 303–7, 1993.

[46] T. Rootwelt, R. Almaas, S. Oyasaeter, A. Moen, and O. D. Saugstad, "Release of xanthine oxidase to the systemic circulation during resuscitation from severe hypoxemia in newborn pigs," *Acta Paediatrica*, vol. 84, no. 5, pp. 507–11, 1995.

[47] K. Huh, I. Yamamoto, E. Gohda, and H. Iwata, "Tissue distribution and characteristics of xanthine oxidase and allopurinol oxidizing enzyme," *Japanese Journal of Pharmacology*, vol. 26, no. 6, pp. 719–24, 1976.

[48] H. Kanemitsu, A. Tamura, T. Kirino, S. Karasawa, K. Sano, T. Iwamoto, M. Yoshiura, and K. Iriyama, "Xanthine and uric acid levels in rat brain following focal ischemia," *Journal of Neurochemistry*, vol. 51, no. 6, pp. 1882–5, 1988.

[49] P. Pacher, A. Nivorozhkin, and C. Szabo, "Therapeutic effects of xanthine oxidase inhibitors: renaissance half a century after the discovery of allopurinol," *Pharmacological Reviews*, vol. 58, no. 1, pp. 87–114, 2006.

[50] R. O. Day, G. G. Graham, M. Hicks, A. J. McLachlan, S. L. Stocker, and K. M. Williams, "Clinical pharmacokinetics and pharmacodynamics of allopurinol and oxypurinol," *Clinical Pharmacokinetics*, vol. 46, no. 8, pp. 623–44, 2007.

[51] Y. Takano, K. Hase-Aoki, H. Horiuchi, L. Zhao, Y. Kasahara, S. Kondo, and M. A. Becker, "Selectivity of febuxostat, a novel non-purine inhibitor of xanthine oxidase/xanthine dehydrogenase," *Life Sciences*, vol. 76, no. 16, pp. 1835–47, 2005.

[52] J. H. Tayar, M. A. Lopez-Olivo, and M. E. Suarez-Almazor, "Febuxostat for treating chronic gout," *Cochrane Database of Systematic Reviews*, vol. 11, p. CD008653, 2012.

[53] U. Z. Malik, N. J. Hundley, G. Romero, R. Radi, B. A. Freeman, M. M. Tarpey, and E. E. Kelley, "Febuxostat inhibition of endothelial-bound xo: implications for targeting vascular ros production," *Free Radical Biology & Medicine*, vol. 51, no. 1, pp. 179–84, 2011.

[54] H. R. Schumacher Jr, M. A. Becker, R. L. Wortmann, P. A. MacDonald, B. Hunt, J. Streit, C. Lademacher, and N. Joseph-Ridge, "Effects of febuxostat versus allopurinol and placebo in reducing serum urate in subjects with hyperuricemia and gout: a 28-week, phase iii, randomized, double-blind, parallel-group trial," *Arthritis Care & Research*, vol. 59, no. 11, pp. 1540–1548, 2008.

[55] K.-H. Yu, "Febuxostat: a novel non-purine selective inhibitor of xanthine oxidase for the treatment of hyperuricemia in gout," *Recent Patents on Inflammation & Allergy Drug Discovery*, vol. 1, no. 1, pp. 69–75, 2007.

[56] W. M. Pardridge, "Drug transport across the blood-brain barrier," *Journal of Cerebral Blood Flow & Metabolism*, vol. 32, no. 11, pp. 1959–72, 2012.

[57] C. Saraiva, C. Praca, R. Ferreira, T. Santos, L. Ferreira, and L. Bernardino, "Nanoparticle-mediated brain drug delivery: Overcoming blood-brain barrier to treat neurodegenerative diseases," *Journal of Controlled Release*, vol. 235, pp. 34–47, 2016.

[58] J. M. Scherrmann, "Drug delivery to brain via the blood-brain barrier," *Vascular Pharmacology*, vol. 38, no. 6, pp. 349–54, 2002.

[59] S. M. Stamatovic, R. F. Keep, and A. V. Andjelkovic, "Brain endothelial cell-cell junctions: how to "open" the blood brain barrier," *Current Neuropharmacology*, vol. 6, no. 3, pp. 179–192, 2008.

[60] H. Wolburg and A. Lippoldt, "Tight junctions of the blood–brain barrier: development, composition and regulation," *Vascular Pharmacology*, vol. 38, no. 6, pp. 323–337, 2002.

[61] L. R. Freeman and J. N. Keller, "Oxidative stress and cerebral endothelial cells: regulation of the blood–brain-barrier and antioxidant based interventions," *Biochimica et Biophysica Acta (BBA) - Molecular Basis of Disease*, vol. 1822, no. 5, pp. 822–829, 2012.

[62] B. Obermeier, R. Daneman, and R. M. Ransohoff, "Development, maintenance and disruption of the blood-brain barrier," *Nature Medicine*, vol. 19, no. 12, p. 1584, 2013.

[63] S. Liebner, R. M. Dijkhuizen, Y. Reiss, K. H. Plate, D. Agalliu, and G. Constantin, "Functional morphology of the blood–brain barrier in health and disease," *Acta Neuropathologica*, pp. 1–26, 2018.

[64] G. J. Schenk and H. E. de Vries, "Altered blood–brain barrier transport in neuroinflammatory disorders," *Drug Discovery Today: Technologies*, vol. 20, pp. 5–11, 2016.

[65] S. Leech, J. Kirk, J. Plumb, and S. McQuaid, "Persistent endothelial abnormalities and blood–brain barrier leak in primary and secondary progressive multiple sclerosis," *Neuropathology and Applied Neurobiology*, vol. 33, no. 1, pp. 86–98, 2007.

[66] J. J. Lochhead, G. McCaffrey, C. E. Quigley, J. Finch, K. M. DeMarco, N. Nametz, and T. P. Davis, "Oxidative stress increases blood–brain barrier permeability and induces alterations in occludin during hypoxia–reoxygenation," *Journal of Cerebral Blood Flow & Metabolism*, vol. 30, no. 9, pp. 1625–1636, 2010.

[67] H. J. van de Haar, S. Burgmans, J. F. Jansen, M. J. van Osch, M. A. van Buchem, M. Muller, P. A. Hofman, F. R. Verhey, and W. H. Backes, "Blood-brain barrier leakage in patients with early alzheimer disease," *Radiology*, vol. 281, no. 2, pp. 527–535, 2016.

[68] M. Fiorentino, A. Sapone, S. Senger, S. S. Camhi, S. M. Kadzielski, T. M. Buie, D. L. Kelly, N. Cascella, and A. Fasano, "Blood–brain barrier and intestinal epithelial barrier alterations in autism spectrum disorders," *Molecular Autism*, vol. 7, no. 1, p. 49, 2016.

[69] N. T Issa, H. Wathieu, A. Ojo, S. W Byers, and S. Dakshanamurthy, "Drug metabolism in preclinical drug development: a survey of the discovery process, toxicology, and computational tools," *Current Drug Metabolism*, vol. 18, no. 6, pp. 556–565, 2017.

[70] O. A. Almazroo, M. K. Miah, and R. Venkataramanan, "Drug metabolism in the liver," *Clinics in Liver Disease*, vol. 21, no. 1, pp. 1–20, 2017.

[71] E. Hedlund, J.-A. Gustafsson, and M. Warner, "Cytochrome p450 in the brain; a review," *Current Drug Metabolism*, vol. 2, no. 3, pp. 245–263, 2001.

[72] V. Ravindranath, H. K. Anandatheerthavarada, and S. K. Shankar, "Nadph cytochrome p-450 reductase in rat, mouse and human brain," *Biochemical Pharmacology*, vol. 39, no. 6, pp. 1013–1018, 1990.

[73] R. Meech and P. I. Mackenzie, "Structure and function of uridine diphosphate glucuronosyltransferases," *Clinical and Experimental Pharmacology and Physiology*, vol. 24, no. 12, pp. 907–915, 1997.

[74] J. G. Wagner, "History of pharmacokinetics," *Pharmacology & Therapeutics*, vol. 12, no. 3, pp. 537–562, 1981.

[75] R. Khosravan, B. Grabowski, J.-T. Wu, N. Joseph-Ridge, and L. Vernillet, "Effect of food or antacid on pharmacokinetics and pharmacodynamics of febuxostat in healthy subjects," *British Journal of Clinical Pharmacology*, vol. 65, no. 3, pp. 355–363, 2008.

[76] Z. Luo, F. Nan, J. Miao, Z. Chen, M. Li, and M. Liang, "Pharmacokinetics and bioequivalence of two formulations of febuxostat 40-mg and 80-mg tablets: a random-

ized, open-label, 4-way crossover study in healthy chinese male volunteers," *PloS One*, vol. 11, no. 3, p. e0150661, 2016.

[77] B. Kamel, G. G. Graham, K. M. Williams, K. D. Pile, and R. O. Day, "Clinical pharmacokinetics and pharmacodynamics of febuxostat," *Clinical Pharmacokinetics*, vol. 56, no. 5, pp. 459–475, 2017.

[78] H. Tatsuo and O. Iwao, "A repeated oral administration study of febuxostat (tmx-67), a non-purine-selective inhibitor of xanthine oxidase, in patients with impaired renal function in japan: pharmacokinetic and pharmacodynamic study," *Journal of Clinical Rheumatology*, vol. 17, no. 4, pp. S27–S34, 2011.

[79] M. Zhang, X. Di, L. Xu, J. Xu, Y. Yang, N. Jiang, L. Song, and X. Xu, "Pharmacokinetics and pharmacodynamics of febuxostat under fasting conditions in healthy individuals," *Experimental and Therapeutic Medicine*, vol. 7, no. 2, pp. 393–396, 2014.

[80] R. Khosravan, B. A. Grabowski, M. D. Mayer, J.-T. Wu, N. Joseph-Ridge, and L. Vernillet, "The effect of mild and moderate hepatic impairment on pharmacokinetics, pharmacodynamics, and safety of febuxostat, a novel nonpurine selective inhibitor of xanthine oxidase," *The Journal of Clinical Pharmacology*, vol. 46, no. 1, pp. 88–102, 2006.

[81] M. Becker, J. Kisicki, R. Khosravan, J. Wu, D. Mulford, B. Hunt, P. MacDonald, and N. Joseph-Ridge, "Febuxostat (tmx-67), a novel, non-purine, selective inhibitor of xanthine oxidase, is safe and decreases serum urate in healthy volunteers," *Nucleosides, Nucleotides and Nucleic Acids*, vol. 23, no. 8-9, pp. 1111–1116, 2004.

[82] M. D. Mayer, R. Khosravan, L. Vernillet, J.-T. Wu, N. Joseph-Ridge, and D. J. Mulford, "Pharmacokinetics and pharmacodynamics of febuxostat, a new non-purine se-

lective inhibitor of xanthine oxidase in subjects with renal impairment," *American Journal of Therapeutics*, vol. 12, no. 1, pp. 22–34, 2005.

[83] R. Khosravan, B. A. Grabowski, J.-T. Wu, N. Joseph-Ridge, and L. Vernillet, "Pharmacokinetics, pharmacodynamics and safety of febuxostat, a non-purine selective inhibitor of xanthine oxidase, in a dose escalation study in healthy subjects," *Clinical Pharmacokinetics*, vol. 45, no. 8, pp. 821–841, 2006.

[84] H. Zhou, Y. Zheng, G. Wu, X. Hu, Y. Zhai, D. Iv, J. Liu, L. Wu, and J. Shentu, "Pharmacokinetics and tolerability of febuxostat after oral administration in healthy chinese volunteers: a randomized, open-label, singleand multiple-dose three-way crossover study," *International Journal of Clinical Pharmacology and Therapeutics*, vol. 54, no. 2, p. 115, 2016.

[85] Y. Wu, Z. Mao, Y. Liu, X. Wang, and X. Di, "Simultaneous determination of febuxostat and its three active metabolites in human plasma by liquid chromatography–tandem mass spectrometry and its application to a pharmacokinetic study in chinese healthy volunteers," *Journal of Pharmaceutical and Biomedical Analysis*, vol. 114, pp. 216–221, 2015.

[86] K.-A. Kim and J.-Y. Park, "Comparison of pharmacokinetics and uric acid lowering effect between two different strength febuxostat formulations (80 mg vs. 40 mg) in healthy subjects.," *International Journal of Clinical Pharmacology and Therapeutics*, vol. 53, no. 8, pp. 667–673, 2015.

[87] H. Tanaka and K. Mizojiri, "Drug-protein binding and blood-brain barrier permeability," *Journal of Pharmacology and Experimental Therapeutics*, vol. 288, no. 3, pp. 912–918, 1999.

[88] R. Nau, F. Sörgel, and H. Eiffert, "Penetration of drugs through the blood-cerebrospinal fluid/blood-brain barrier for treatment of central nervous system infections," *Clinical Microbiology Reviews*, vol. 23, no. 4, pp. 858–883, 2010.

[89] H. Mandula, J. M. R. Parepally, R. Feng, and Q. R. Smith, "Role of site-specific binding to plasma albumin in drug availability to brain," *Journal of Pharmacology and Experimental Therapeutics*, vol. 317, no. 2, pp. 667–675, 2006.

[90] J. Lombard, "Once upon a time the cell membranes: 175 years of cell boundary research," *Biology Direct*, vol. 9, p. 32, 2014.

[91] D. M. Owen, K. Gaus, A. I. Magee, and M. Cebecauer, "Dynamic organization of lymphocyte plasma membrane: lessons from advanced imaging methods," *Immunology*, vol. 131, no. 1, pp. 1–8, 2010.

[92] M. B. Stone, S. A. Shelby, and S. L. Veatch, "Super-resolution microscopy: shedding light on the cellular plasma membrane," *Chemical Reviews*, vol. 117, no. 11, pp. 7457–7477, 2017.

[93] P. J. Thornalley, "Isothiocyanates: mechanism of cancer chemopreventive action," *Anticancer Drugs*, vol. 13, no. 4, pp. 331–8, 2002.

[94] X. Wu, Q.-H. Zhou, and K. Xu, "Are isothiocyanates potential anti-cancer drugs?," *Acta Pharmacologica Sinica*, vol. 30, no. 5, pp. 501–12, 2009.

[95] J. V. Cross, F. W. Foss, J. M. Rady, T. L. Macdonald, and D. J. Templeton, "The isothiocyanate class of bioactive nutrients covalently inhibit the mekk1 protein kinase," *BMC Cancer*, vol. 7, p. 183, 2007.

[96] F. S. Hanschen, N. Bruggemann, A. Brodehl, I. Mewis, M. Schreiner, S. Rohn, and L. W. Kroh, "Characterization of products from the reaction of glucosinolate-derived

isothiocyanates with cysteine and lysine derivatives formed in either model systems or broccoli sprouts," *Journal of Agricultural and Food Chemistry*, vol. 60, no. 31, pp. 7735–45, 2012.

[97] C. Ioannides and N. Konsue, "A principal mechanism for the cancer chemopreventive activity of phenethyl isothiocyanate is modulation of carcinogen metabolism," *Drug Metabolism Reviews*, vol. 47, no. 3, pp. 356–73, 2015.

[98] L. Mi, X. Wang, S. Govind, B. L. Hood, T. D. Veenstra, T. P. Conrads, D. T. Saha, R. Goldman, and F. L. Chung, "The role of protein binding in induction of apoptosis by phenethyl isothiocyanate and sulforaphane in human non-small lung cancer cells," *Cancer Research*, vol. 67, no. 13, pp. 6409–16, 2007.

[99] Y. Ji and M. E. Morris, "Membrane transport of dietary phenethyl isothiocyanate by abcg2 (breast cancer resistance protein)," *Molecular Pharmaceutics*, vol. 2, no. 5, pp. 414–9, 2005.

[100] Y. Zhang, "Molecular mechanism of rapid cellular accumulation of anticarcinogenic isothiocyanates," *Carcinogenesis*, vol. 22, no. 3, pp. 425–31, 2001.

[101] Y. Zhang and P. Talalay, "Mechanism of differential potencies of isothiocyanates as inducers of anticarcinogenic phase 2 enzymes," *Cancer Research*, vol. 58, no. 20, pp. 4632–9, 1998.

[102] A. V. Filatov, G. I. Krotov, V. G. Zgoda, and Y. Volkov, "Fluorescent immunoprecipitation analysis of cell surface proteins: a methodology compatible with mass-spectrometry," *Journal of Immunological Methods*, vol. 319, no. 1-2, pp. 21–33, 2007.

[103] H. Maeda, N. Ishida, H. Kawauchi, and K. Tsujimura, "Reaction of fluorescein-isothiocyanate with proteins and amino acids. i. covalent and non-covalent binding

of fluorescein-isothiocyanate and fluorescein to proteins," *Journal of Biochemistry*, vol. 65, no. 5, pp. 777–83, 1969.

[104] S. Miyata and S. Morita, "A new method for visualization of endothelial cells and extravascular leakage in adult mouse brain using fluorescein isothiocyanate," *Journal of Neuroscience Methods*, vol. 202, no. 1, pp. 9–16, 2011.

[105] J. D. Aplin and R. C. Hughes, "Modification of fibroblast surface amines alters receptor-mediated cell spreading on protein-coated substrata but not adsorptive endocytosis," *Journal of Cell Science*, vol. 49, pp. 283–97, 1981.

[106] T. D. Butters, V. Devalia, J. D. Aplin, and R. C. Hughes, "Inhibition of fibronectin-mediated adhesion of hamster fibroblasts to substratum: effects of tunicamycin and some cell surface modifying reagents," *Journal of Cell Science*, vol. 44, pp. 33–58, 1980.

[107] E. C. Butcher and I. L. Weissman, "Direct fluorescent labeling of cells with fluorescein or rhodamine isothiocyanate. i. technical aspects," *Journal of Immunological Methods*, vol. 37, no. 2, pp. 97–108, 1980.

[108] L. M. Jerry and A. K. Sullivan, "The lymphocyte plasma membrane: locus of control in the immune response," *In Vitro*, vol. 12, no. 3, pp. 236–59, 1976.

[109] L. Spotl, A. Sarti, M. P. Dierich, and J. Most, "Cell membrane labeling with fluorescent dyes for the demonstration of cytokine-induced fusion between monocytes and tumor cells," *Cytometry*, vol. 21, no. 2, pp. 160–9, 1995.

[110] M. Kaya and B. Ahishali, "Assessment of permeability in barrier type of endothelium in brain using tracers: Evans blue, sodium fluorescein, and horseradish peroxidase," *Methods in Molecular Biology*, vol. 763, pp. 369–82, 2011.

[111] O. V. Braginskaja, V. V. Lazarev, I. N. Pershina, K. V. Petrov, L. B. Rubin, and O. V. Tikhonova, "Sodium fluorescein accumulation in cultured cells," *General Physiology and Biophysics*, vol. 12, no. 5, pp. 453–64, 1993.

[112] P. Breeuwer, J. L. Drocourt, N. Bunschoten, M. H. Zwietering, F. M. Rombouts, and T. Abee, "Characterization of uptake and hydrolysis of fluorescein diacetate and carboxyfluorescein diacetate by intracellular esterases in saccharomyces cerevisiae, which result in accumulation of fluorescent product," *Applied and Environmental Microbiology*, vol. 61, no. 4, pp. 1614–9, 1995.

[113] K. K. Meisingset and H. B. Steen, "Intracellular binding of fluorescein in lymphocytes," *Cytometry*, vol. 1, no. 4, pp. 272–8, 1981.

[114] G. M. Cooper, *The Cell - A Molecular Approach 2nd Edition.* Sunderland (MA): Sinauer Associates, 2000.

[115] H. Lodish, A. Berk, S. L. Zipursky, P. Matsudaira, D. Baltimore, and J. Darnell, *Molecular Cell Biology*, vol. 29. WH Freeman New York, 2000.

[116] S. M. Zehnder, M. Suaris, M. M. Bellaire, and T. E. Angelini, "Cell volume fluctuations in mdck monolayers," *Biophysical Journal*, vol. 108, no. 2, pp. 247–50, 2015.

[117] D. Bettega, P. Calzolari, S. M. Doglia, B. Dulio, L. Tallone, and A. M. Villa, "Technical report: Cell thickness measurements by confocal fluorescence microscopy on c3h10t1/2 and v79 cells," *International Journal of Radiation Biology*, vol. 74, no. 3, pp. 397–403, 1998.

[118] M. F. Stins, F. Gilles, and K. S. Kim, "Selective expression of adhesion molecules on human brain microvascular endothelial cells," *Journal of Neuroimmunology*, vol. 76, no. 1-2, pp. 81–90, 1997.

[119] A. Chauhan, F. Gu, M. M. Essa, J. Wegiel, K. Kaur, W. T. Brown, and V. Chauhan, "Brain region-specific deficit in mitochondrial electron transport chain complexes in children with autism," *Journal of Neurochemistry*, vol. 117, no. 2, pp. 209–220, 2011.

[120] A. Chauhan, T. Audhya, and V. Chauhan, "Brain region-specific glutathione redox imbalance in autism," *Neurochemical Research*, vol. 37, no. 8, pp. 1681–1689, 2012.

[121] D. A. Rossignol and R. E. Frye, "Evidence linking oxidative stress, mitochondrial dysfunction, and inflammation in the brain of individuals with autism," *Frontiers in Physiology*, vol. 5, p. 150, 2014.

[122] E. M. Sajdel-Sulkowska, M. Xu, and N. Koibuchi, "Increase in cerebellar neurotrophin-3 and oxidative stress markers in autism," *Cerebellum*, vol. 8, no. 3, pp. 366–372, 2009.

[123] E. M. Sajdel-Sulkowska, M. Xu, W. McGinnis, and N. Koibuchi, "Brain region-specific changes in oxidative stress and neurotrophin levels in autism spectrum disorders (asd)," *Cerebellum*, vol. 10, no. 1, pp. 43–48, 2011.

[124] R. Loperena and D. G. Harrison, "Oxidative stress and hypertensive diseases," *Medical Clinics*, vol. 101, no. 1, pp. 169–193, 2017.

[125] S. Abadeh, J. Killacky, M. Benboubetra, and R. Harrison, "Purification and partial characterization of xanthine oxidase from human milk," *Biochimica et Biophysica Acta (BBA)-General Subjects*, vol. 1117, no. 1, pp. 25–32, 1992.

[126] T. Ohtsubo, I. I. Rovira, M. F. Starost, C. Liu, and T. Finkel, "Xanthine oxidoreductase is an endogenous regulator of cyclooxygenase-2," *Circulation Research*, vol. 95, no. 11, pp. 1118–1124, 2004.

[127] D. N. Granger and P. R. Kvietys, "Reperfusion injury and reactive oxygen species: the evolution of a concept," *Redox Biology*, vol. 6, pp. 524–551, 2015.

[128] M. E. Suarez-Almazor, M. A. Lopez-Olivo, and J. H. Tayar, "Febuxostat for treating chronic gout," *Cochrane Database of Systematic Reviews*, no. 8, 2010.

[129] J. L. Silverman, M. Yang, C. Lord, and J. N. Crawley, "Behavioural phenotyping assays for mouse models of autism," *Nature Reviews Neuroscience*, vol. 11, no. 7, p. 490, 2010.

[130] J. N. Crawley, "Designing mouse behavioral tasks relevant to autistic-like behaviors," *Mental Retardation and Developmental Disabilities Research Reviews*, vol. 10, no. 4, pp. 248–258, 2004.

[131] H. G. McFarlane, G. Kusek, M. Yang, J. Phoenix, V. Bolivar, and J. Crawley, "Autism-like behavioral phenotypes in btbr t+ tf/j mice," *Genes, Brain and Behavior*, vol. 7, no. 2, pp. 152–163, 2008.

[132] M. Yang, D. N. Abrams, J. Y. Zhang, M. D. Weber, A. M. Katz, A. M. Clarke, J. L. Silverman, and J. N. Crawley, "Low sociability in btbr t+ tf/j mice is independent of partner strain," *Physiology & Behavior*, vol. 107, no. 5, pp. 649–662, 2012.

[133] M. L. Scattoni, S. U. Gandhy, L. Ricceri, and J. N. Crawley, "Unusual repertoire of vocalizations in the btbr t+ tf/j mouse model of autism," *PloS One*, vol. 3, no. 8, p. e3067, 2008.

[134] B. Pearson, R. Pobbe, E. Defensor, L. Oasay, V. Bolivar, D. Blanchard, and R. Blanchard, "Motor and cognitive stereotypies in the btbr t+ tf/j mouse model of autism," *Genes, Brain and Behavior*, vol. 10, no. 2, pp. 228–235, 2011.

[135] B. A. Babineau, M. Yang, R. F. Berman, and J. N. Crawley, "Low home cage social behaviors in btbr t+ tf/j mice during juvenile development," *Physiology & Behavior*, vol. 114, pp. 49–54, 2013.

[136] S. S. Moy, J. J. Nadler, N. B. Young, A. Perez, L. P. Holloway, R. P. Barbaro, J. R. Barbaro, L. M. Wilson, D. W. Threadgill, J. M. Lauder, *et al.*, "Mouse behavioral tasks relevant to autism: phenotypes of 10 inbred strains," *Behavioural Brain Research*, vol. 176, no. 1, pp. 4–20, 2007.

[137] W. A. Banks, "Characteristics of compounds that cross the blood-brain barrier," *BMC Neurology*, vol. 9, no. 1, p. S3, 2009.

[138] W. A. Banks, "Developing drugs that can cross the blood-brain barrier: applications to alzheimer's disease," *BMC Neuroscience*, vol. 9, no. 3, p. S2, 2008.

[139] T. Tan, S. W. Watts, and R. P. Davis, "Drug delivery: enabling technology for drug discovery and development. iprecio® micro infusion pump: programmable, refillable and implantable," *Frontiers in Pharmacology*, vol. 2, p. 44, 2011.

[140] S. A. Grathwohl and M. Jucker, "Replacement of osmotic minipumps to extend the intracerebral infusion time of compounds into the mouse brain," *Biotechniques*, vol. 55, no. 2, pp. 75–78, 2013.

[141] H. Naik, J.-t. Wu, R. Palmer, and L. McLean, "The effects of febuxostat on the pharmacokinetic parameters of rosiglitazone, a cyp2c8 substrate," *British Journal of Clinical Pharmacology*, vol. 74, no. 2, pp. 327–335, 2012.

[142] M. Mukoyoshi, S. Nishimura, S. Hoshide, S. Umeda, M. Kanou, K. Taniguchi, and H. Muroga, "In vitro drug–drug interaction studies with febuxostat, a novel non-purine selective inhibitor of xanthine oxidase: plasma protein binding, identification of metabolic enzymes and cytochrome p450 inhibition," *Xenobiotica*, vol. 38, no. 5, pp. 496–510, 2008.

[143] F. Dutheil, P. Beaune, and M.-A. Loriot, "Xenobiotic metabolizing enzymes in the

central nervous system: Contribution of cytochrome p450 enzymes in normal and pathological human brain," *Biochimie*, vol. 90, no. 3, pp. 426–436, 2008.

[144] C. S. Ferguson and R. F. Tyndale, "Cytochrome p450 enzymes in the brain: emerging evidence of biological significance," *Trends in Pharmacological Sciences*, vol. 32, no. 12, pp. 708–714, 2011.

[145] D. Hira, Y. Chisaki, S. Noda, H. Araki, T. Uzu, H. Maegawa, Y. Yano, S.-y. Morita, and T. Terada, "Population pharmacokinetics and therapeutic efficacy of febuxostat in patients with severe renal impairment," *Pharmacology*, vol. 96, no. 1-2, pp. 90–98, 2015.

[146] T. Hirai, T. Kimura, and H. Echizen, "Modeling and simulation for estimating the influence of renal dysfunction on the hypouricemic effect of febuxostat in hyperuricemic patients due to overproduction or underexcretion of uric acid," *Biological and Pharmaceutical Bulletin*, vol. 39, no. 6, pp. 1013–1021, 2016.

[147] B. R. Chandu, K. Kanala, N. T. Hwisa, P. Katakam, and M. Khagga, "Bioequivalance and pharmacokinetic study of febuxostat in human plasma by using lc-ms/ms with liquid liquid extraction method," *SpringerPlus*, vol. 2, no. 1, p. 194, 2013.